STANFORD RESEARCH INSTITUTE
MENLO PARK, CALIFORNIA

October 1963

Technical Report 2

MEDIUM RESOLUTION INFRARED (MRIR) AND HIGH RESOLUTION INFRARED (HRIR) DATA PROCESSING AND CONVERSION

Prepared for:

NATIONAL AERONAUTICS AND SPACE ADMINISTRATION
GODDARD SPACE FLIGHT CENTER
GREENBELT, MARYLAND

CONTRACT NAS 5-1882

By: H. Frohbach R. M. Madvig R. L. Mancuso M. Pollack

SRI Project No. 3927

Approved:

E. B. SHAPIRO, ACTING MANAGER SYSTEMS ENGINEERING LABORATORY

J. D. NOE, DIRECTOR ENGINEERING SCIENCES DIVISION

D. R. SCHEUCH, DIRECTOR ELECTRONICS AND RADIO SCIENCES DIVISION

Copy No. 37

PREFACE

This report combines into one report the reporting requirements of Item 5 and Item 6 of the contract. Item 5 is a report on analysis of the characteristics of MRIR data for processing at the CDA station and Item 6 is a report on the feasibility of converting MRIR and HRIR data into units of physical significance at the CDA station. These two subjects were found to be inseparable and are, therefore, reported together.

ABSTRACT

~~16705~~ 16705

A

The Nimbus satellite instrumentation includes a five-channel infrared radiometer, each channel of which is sensitive to a different spectral region. The radiometer scans a swath of the earth extending to the horizon on each side of the path of the satellite. The infrared sensors will each have a resolution of about 24 miles on the earth's surface and the term Medium Resolution Infrared (MRIR) is applied to the system and to the data.

The satellite also has a single channel High Resolution Infrared Radiometer (HRIR) that scans the earth in the same manner as the MRIR radiometer but with a resolution of about 5 miles on the earth's surface.

This report discusses the operational use of the MRIR and HRIR data, and methods for preparing the data for use by operational meteorologists. A cartographic data format is recommended and methods of showing the MRIR as contours, varying gray shades, and number symbols are discussed in the report. A method for rectification of the data into standard map projections such as polar stereographic in real time by means of a digital computer is described.

AUTHOR

CONTENTS

CONTENTS

ILLUSTRATIONS

ILLUSTRATIONS

ILLUSTRATIONS

TABLES

I INTRODUCTION

The report presents the work accomplished under Tasks 3 and 4 of Contract NAS5-1882. The reason for combining the work under the two tasks is that data processing requirements and the conversion of data to units of physical significance are too tightly interwoven to be considered as separate subjects.

Section II of the report summarizes the conclusions of the work. Section III discusses the operational uses of the MRIR data and the conversion of MRIR and HRIR data into units of physical significance. Section IV is concerned with the form of presentation of the MRIR data. Various cartographic presentations are described, and the preferred method (one that uses gray scale plus numeric data) is shown as having the best potential. Examples are illustrated using TIROS window channel data. Section V describes a hardware configuration that processes the raw MRIR data into video data which, when printed by a standard facsimile printer, yields the preferred presentation. Section VI discusses the advantages of rectifying the MRIR data and the accuracy requirements for both gridding and rectification, summarizes some other efforts (not from SRI) to solve the general problem of digital rectification of pictorial data, proposes an inverse approach to rectification, and discusses the pros and cons of the orthodox versus the inverse method, provides a background description of the nature of the unrectified data and the rectified picture, and finally presents three inverse methods for rectification and tentatively recommends one as the best method. Appendices A and B describe limb darkening and scattering of the solar radiation, their effects on the meaning of the data, and computations for corrections.

II TENTATIVE RECOMMENDATIONS FOR PROCESSING OF MRIR AND HRIR DATA

The MRIR instrument package is not scheduled to be included on the first few Nimbus satellites. Since there may be some changes in the radiometer design before the MRIR becomes operational, only tentative recommendations are made in this report.

A. Recommendations for Processing MRIR Data

1. For operational use, the data should be presented in a cartographic form.

2. The data should be gridded by marking points spaced along standard longitude and latitude lines. Every 10 degrees of longitude and latitude should be marked in the equatorial and mid-latitudes. The interval should be increased between the lines of longitude near the poles to avoid cluttering the pictures. The points chosen along these lines should be spaced every 1 or 2 degrees, except near the poles where the spacing along the parallels should be decreased to avoid cluttering.

3. The MRIR data in its natural or raw form consists of a set of contiguous scan lines of the earth's surface and atmosphere; these data could therefore be printed on a standard facsimile printer. If printed on a 100-line-to-the-inch printer, the resulting "picture" would be 0.36 inch wide by 3.6 inches long. Since this is much too small for practical use, it is recommended that the data should be stretched electronically, before transmission, to a size more suited to operational use. An increase of 10:1 or 20:1 in linear dimensions is required.

4. It is recommended that the MRIR picture be portrayed by means of gray shading with numbers superimposed. Gray shading facilitates seeing the general pattern of high-, intermediate-, and low-energy regions and the superimposed numbers make it possible to accurately

present the parameter values. A simulated presentation is shown in Figs. 13 and 14, pages 35 and 36. A data processing system that would convert the MRIR data into this gray level plus number format was designed and is shown in block diagram form in Fig. 17, page 40. The hardware required to build this system is all within the present state of the art.

5. The window channel measurements would be more useful if converted to effective radiation temperature. The effects of limb darkening on this channel in Nimbus will be negligible, so that the conversion can be made easily.

6. Rectification of the MRIR data by means of the CDC 924 computer in real-time appears to be feasible by means of a method described in Section VI. Verification of the feasibility should be made and, if it is possible, it is recommended that the MRIR data be converted to polar stereographic projections of the northern and southern hemispheres.

B. Recommendations for Processing HRIR Data

1. The HRIR data should be gridded by marking points along standard longitude and latitude lines as recommended for the MRIR data. Two mathematical models for performing the gridding computations in real time on the CDC 924 computer were reported in Technical Report 1 of this series, entitled "High Resolution Infrared (HRIR) Gridding."

2. The HRIR data should be presented as a gray-level gridded picture in its unrectified form, in accordance with present NASA planning for CDA data processing. Rectification in real time by means of the CDC 924 computer, while it appears feasible for the MRIR, does not appear feasible for the HRIR, since the number of HRIR data points far exceeds the number of MRIR data points. Conversion of HRIR data into units of physical significance is not recommended.

3. Electronic stretching of the HRIR data to fit a larger area is not as important a requirement as stretching the MRIR although it is feasible. The unstretched picture would be only about 2.5 inches

wide, printed 100 lines per inch. Electronic stretching by a linear factor of three is recommended. Three is a convenient enlargement as the data would then fit onto a standard 8-inch printer.

4. Extensive processing of HRIR is not recommended until after experience with the data; e.g., not until after the first HRIR radiometer has been "flown" and the HRIR data has been studied.

III OPERATIONAL APPLICATIONS OF NIMBUS MRIR AND HRIR DATA

A. MRIR Data

1. With the introduction of the meteorological satellites, the expected value of television cloud pictures was confirmed. More recently, the medium resolution infrared radiation (MRIR) data are of a different kind than the television pictures. The television system provides a high resolution portrayal of clouds by their patterns; the exact light value or energy received is not measured precisely in amplitude. The MRIR employs a coarse resolution that will not reveal or convey fine patterns but provides a more accurate measurement than television can of the energy intensity in five spectral regions. Therefore, the Nimbus MRIR data can be expected to be used operationally in a different manner than data from the Nimbus Advanced Vidicon Camera System (AVCS). For many purposes, the loss in detail resulting from the use of MRIR is consistent with analysis and forecasting procedures. Detailed features of clouds are short-lived and what is seen at one moment will have changed within the hour. It is the larger synoptic patterns--cloud arrangements with dimensions of hundreds of miles--which persist and give information compatible with numerical techniques. TIROS data have shown that these larger features of clouds are excellently portrayed both in time and space by the medium resolution data. Also, these MRIR quantitative data are immediately amenable to numerical processing and manipulation. One may suspect that meteorologists will find it much more convenient to develop relationships between MRIR quantitative information and numerical analysis and prediction techniques than between AVCS and the numerical procedures. Since the importance of numerical procedures of forecasting is increasing, it is possible that the use of MRIR data will increase concurrently, as basic technological links are established.

In order to consider the operational applications of Nimbus MRIR data it will be of benefit to mention briefly the TIROS system which was designed to pave the way for more advanced systems such as the Nimbus. The NASA TIROS satellites II, III, and IV have each contained a five-channel, scanning, MRIR instrument unit. Some of the characteristics and potential applications of the five MRIR channels have been tabulated in Table I. Demonstrations of the success of the TIROS II experiment have been given by Bandeen et al.[1]* and by Hanel and Stroud,[2] both in 1961, by Fritz and Winston[3] in 1962, and by Rao and Winston[4] in 1963; preliminary results for TIROS III were presented by Nordberg et al.[5] in 1962. Wark et al.[6] have conducted some successful theoretical experiments (published in 1962) that pertain to infrared flux and surface temperature determinations for TIROS II, III, and IV.

Although the TIROS radiation measuring platforms have shown considerable preliminary success, it is the Nimbus satellites that will provide meteorologists with an operational system. The Nimbus satellite will describe a near polar and circular orbit about the earth at about either local noon or midnight. It will circulate the earth roughly 14 times per day and will provide meteorologists with a complete day and night coverage of the earth every 24 hours. The Nimbus MRIR system will use channels (Table I) similar to those of the TIROS II. One important difference in the spectrums is that the window channel is to respond to a narrower spectral wavelength interval (10-11 microns); consequently there will be less atmospheric absorption of the energy emitted by the viewed surfaces. Also, an improved scanning geometry for the Nimbus MRIR instrument will make the data much easier to prepare for use; that is, gridding and rectifying will be very much easier to perform. All of the earth will be viewed at reasonable nadir angles and overlapping data gathered for high nadir angles probably will be ignored.

* References are listed at the end of the report.

Table I

MRIR CHARACTERISTICS AND APPLICATIONS

NIMBUS +		TIROS III ++		Type of Radiation*	Examples of Applications When Combined with Additional Information
Channel No.	Spectral Response (microns)	Channel No.	Spectral Response (microns)		
1	6.6 - 7.0	1	6.0 - 6.6	Emitted: covers principal part of the 6.3-micron water vapor absorption band	Atmospheric water vapor (Unsubstantiated)
2	10.0 - 11.0	2	7.5 - 13.5	Emitted: covers window region of minimum water vapor absorption	Surface and cloud top temps. Cloud amount and top heights Planetary infrared emission
3	0.6 - 0.75	5	0.5 - 0.75	Reflected: covers scattered and reflected visible solar radiation	Visible reflectance Cloud amount and thickness Terrain features
4	7.5 - 30.0	4	7.5 - 32.0	Emitted: covers 80 percent of emitted thermal radiation	Planetary infrared emission
5	0.2 - 4.0	3	0.2 - 6.0	Reflected: covers scattered and reflected total solar radiation	Planetary solar reflectance

+ NIMBUS characteristics: 2.8 degree instantaneous field of view; 8 rpm scan rate; information bandwidth of 8 cps.

++ TIROS characteristics: 5 degree field of view; 12 rpm spin rate; information bandwidth of 8 cps.

* Radiation emitted by the earth is observable throughout the day while that reflected is observable only during daylight hours.

In the following discussion the most directly usable of the MRIR channels--the window channel--will be described in view of its applications and limitations as deduced from the TIROS experiments. Data from the visible channel will also be considered to some degree because, of their potential value when used in combination with the window data. Only a brief consideration has been given to the other channels because existing operational systems are not designed for their application at this time.

2. Operational Applications

Of the various infrared channels, the operational value of the window channel is most widely and best understood. The results of the work on this one channel may apply to the other channels, particularly the work on data presentation (Section IV). Consequently, the emphasis in the following discussion will be placed upon this particular channel.

In working with the window data of the TIROS experiments, it has been found practical to express the data in terms of an effective temperature of a blackbody radiator instead of the emitted energy flux. A detailed description of the governing relationship between these two quantities is given in the TIROS III Radiation Data-Users Manual published by NASA in 1963. Once the complicated calibration of the instrument has been performed, the data may be easily placed in either form. The significance of the effective temperature presentation is that the data (window) immediately provides an approximation to the temperature of the emitting ground surface or cloud top. The discrepancies which occur between the measured effective temperatures and the true emitting surface temperatures in TIROS data are largely due to the effect of water vapor and ozone absorption. For TIROS this depletion of surface emittance produced temperature differences as large as 10°C or even greater in the case of a high angular view. The narrower window of Nimbus and the fact that the entire earth will be viewed at reasonable nadir angles should diminish this discrepancy.

An example of the effective temperatures obtained from TIROS III, Pass 3, 12 July 1961 is shown in Fig. 1(a) in conjunction with a simultaneous television cloud picture. Although these two sources of data are of a different nature, it is seen that by use of the window data itself, the areas of extensive cloudiness (cold) may be distinguished roughly from the cloudless areas (warm). This effect is more vividly noticeable by comparing the continuous gray picture for the window data with a rectified drawing produced from several television pictures (Fig. 2).

Cloud top height can be obtained by assuming that the effective temperature is the cloud top temperature and referring to temperature versus height information from radiosonde or climatological data. Cloud heights were computed in this manner (using radiosonde data) for Pass 3 of TIROS III and are shown in the overlay of Fig. 2. The results, which reflect the original Channel 2 data, suggest that a slight change in position might be needed to compensate for possible location errors.

Wherever the cloud cover is not a uniform overcast, as in the case of cumulus activity, the radiometer reading also includes the effect of energy received partially from the cloud and partially from the earth's surface or from a lower cloud deck. Also, an important limb-darkening effect occurs for partial cloudiness conditions (Appendix A). These effects are not accounted for in Fig. 2, but in future applications the data may be improved by adjusting according to the percentage and type of cloud cover (obtained from high resolution information) or by a combined utilization of the visible and window channel (discussed later). Also, the Nimbus MRIR resolution element will be approximately a quarter of the size (area) of the TIROS resolution element. Therefore, the Nimbus radiometer will be able to resolve smaller cloud elements than TIROS, so that some of the difficulties due to partial cloudiness will occur somewhat less often with Nimbus than with TIROS. Neglected in the computations of these cloud top heights was the effect due to water vapor and ozone. As mentioned previously, this effect will not be as serious with the Nimbus as it was with TIROS, and approximate corrections

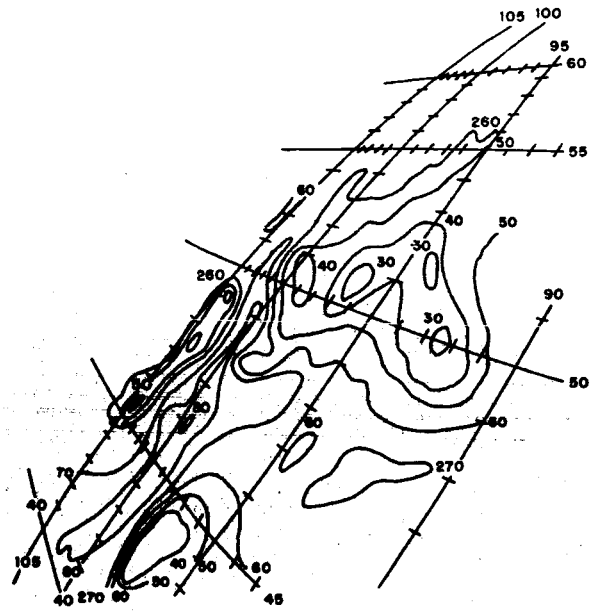

CHANNEL 2
(a)

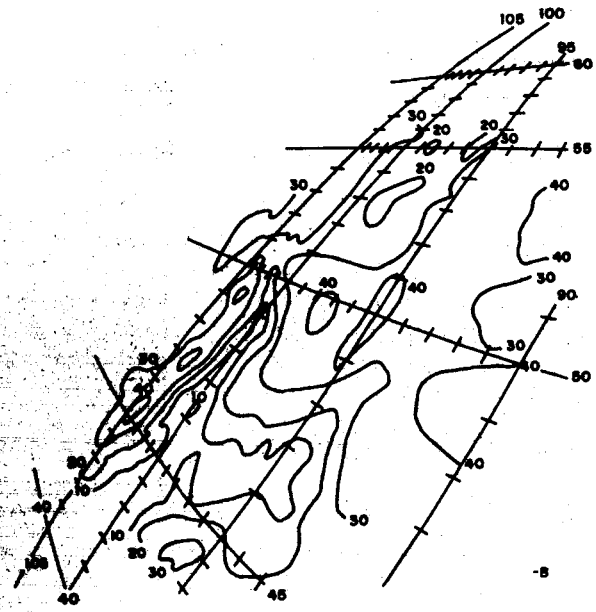

CHANNEL 5
(b)

CHANNEL 2

(c)

CHANNEL 5

(d)

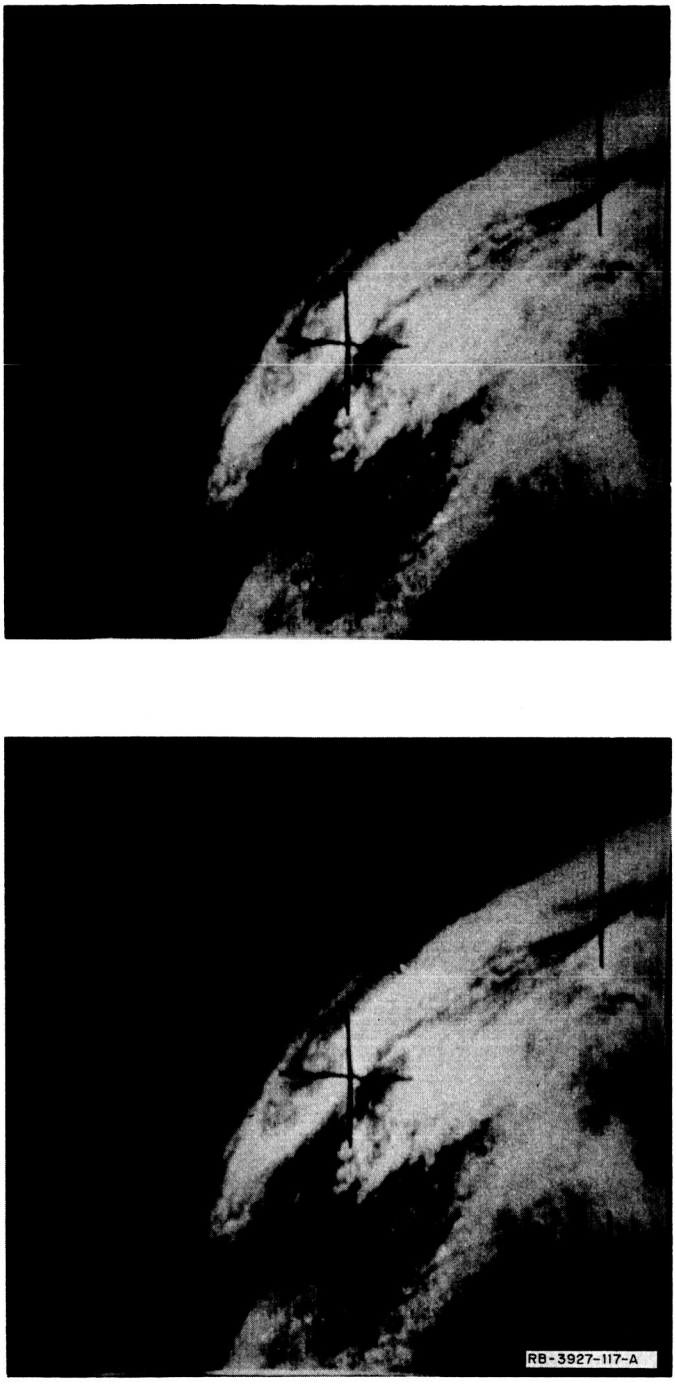

FIG. 1 GRIDDED CLOUD PHOTOGRAPH – TIROS III, PASS 3, 12 JULY 1961, 1548Z
(a) Top Overlay: Isopleths (°K) of Channel 2 MRIR Data – 1540-47Z
(b) Bottom Overlay: Isopleths (watts/m^2) of Channel 5 MRIR Data

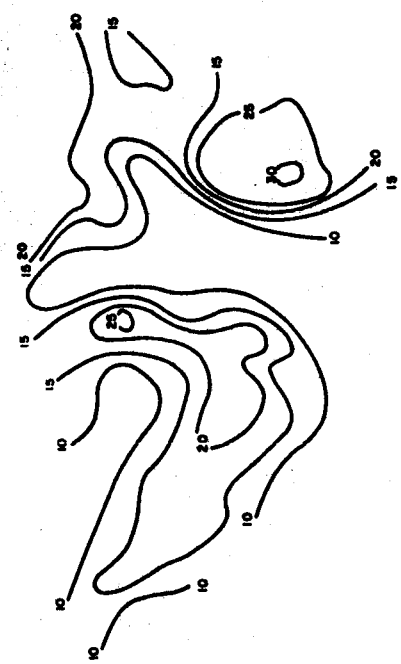
20
15
15
25
20
15
0
20
15
25
15
0
20
10
10
10
0

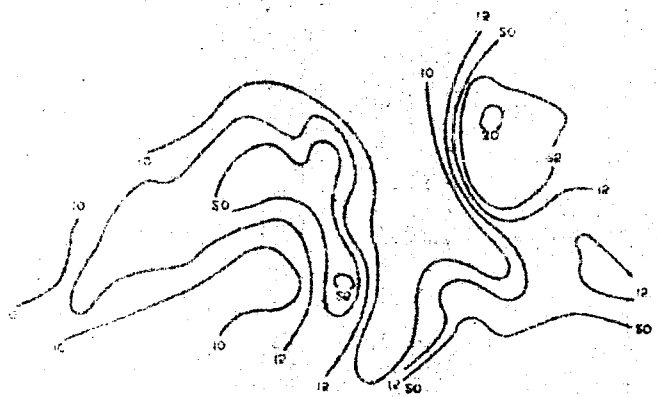
12
50
10
20
30
12
10
50
20
12
10
50
10
12
12
12
50

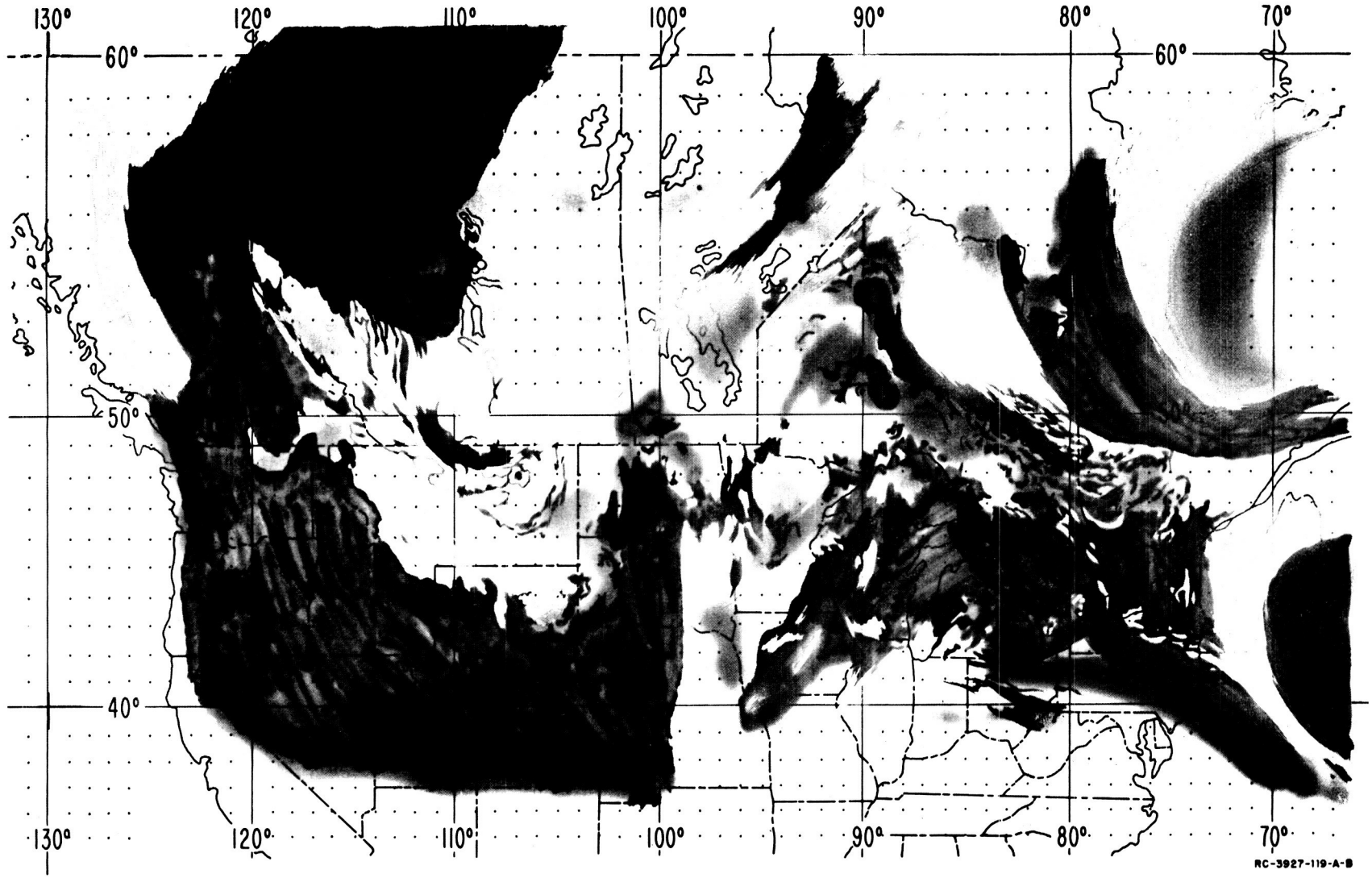

FIG. 2 RECTIFICATION OF SEVERAL CLOUD PHOTOGRAPHS – 12 JULY 1961, 1547-53Z
(Overlay: MRIR-Deduced Cloud-Top Heights, in thousands of feet, 1540-47Z)

could be easily incorporated into an automatic computational scheme. Also, the neglect of the effects of increased water vapor absorption when viewing at high nadir angles will in general not introduce appreciable errors. (Table A-1 shows the calculated error for TIROS III due to this limb darkening.) These errors--which would be smaller for Nimbus--are only significant for extremely high temperatures and high nadir angles. In the case of the Nimbus, measurements with high nadir angles (above 55 degrees) could be ignored because the satellite will obtain a full earth coverage with nadir angles within 55 degrees. Unfortunately, no satisfactory means existed to examine quantitatively the results (Fig. 2) and the relative significance of the various assumptions. Since conventional surface observations do not even include an estimate of cloud top heights, information is only present to the extent that cloud tops can be deduced from reports of cloud bases and types. For example, a report of towering cumulus might indicate tops somewhere between 15,000 and 35,000 feet.

Rao and Winston[4] also computed cloud top heights in a similar way, but included an approximate correction for water vapor and ozone. They found that these cloud top heights were at least in general agreement with heights deduced from conventional data and some aircraft observations. It would be desirable to gain more knowledge of the effectiveness of the window channel for height determination by means of an experimental program which allowed quantitative comparison of satellite radiation data with simultaneously scheduled aircraft observations. Regardless of the existing research needs, however, the window channel is providing valuable cloud information which normally is unavailable to the operational meteorologist.

Many of the problems involved in the computation of a cloud top temperature (or height) naturally carry over to the estimation of the earth's surface temperature. Ironically, verification of these MRIR-deduced surface temperatures is about as difficult as the verification of cloud top heights. Direct measurements of this quantity are very difficult and normal meteorological surface temperatures refer to air measurements performed several feet above this surface.

A fully automatic, real-time system based on stored climatological data could easily be developed for converting effective temperatures to estimated cloud top heights or ground surface temperatures. A simple but effective means based on the results of Wark et al.[6] could be made for taking into account the normal absorption by water vapor and ozone. Because of errors in the climatological data, the procedure would have an uncertainty of about one kilometer for cloud top heights and about 5°C for surface temperatures. However, the presentation of window data in terms of cloud top heights or surface temperatures in this manner does not appear necessary or advisable for the preliminary systems. A presentation (to operational users) of the effective temperatures supplemented with other observations and a climatological manual would appear to be the most practical manner for interpreting the window data of the initial Nimbus experiments.

Probably some of the discrepancies intrinsic in the window data may be resolved by combining data from the window with data from the visible channel. This may allow the distinction of cloud types such as thin cirrus and cumulus activity, or of terrain features such as snow and mountains. In contrast to that of the window, the response of the visible channels represents a measurement of the energy flux scattered and reflected by the viewed area. Naturally the measurements will only be available during the daylight part of the Nimbus orbit. An example of the TIROS III visible flux measurement is shown in the overlay of Fig. 1(b). As can be seen, it is in excellent qualitative agreement with the underlying television cloud picture.

For operational purposes, the user will probably prefer that the visible channel data be presented in terms of a reflectance.* The conversion of the measured flux into reflectance is dependent on the solar flux incident on the viewed area (solar elevation angle) and on the scattering geometry. A planetary isotropic reflectance--dependent only on the solar elevation angle--could easily be computed automatically

* The ratio of the radiant energy scattered and reflected from a surface to the energy incident upon it in the given spectral interval.

in the Nimbus presentation system. It is believed that this would be the best method of treating the Nimbus visible data. Neglect of the dependence on the scattering geometry may affect absolute values, but should not seriously distort the reflectance across synoptic scale patterns. This is partially due to the fact that with the Nimbus system there will only be backward directed scattering, that is, scattering angles between 90° (at poles) and 180° (at equator), as discussed in Appendix B. Consequently, the Nimbus visible data could not, as could the TIROS, contain a mixture which included the strong peaking of forward scattering.

In order to investigate the potential of combining window and visible data, a comparison was made of measured MRIR data (TIROS III, Pass 3) with simultaneous surface observations. The results are summarized in Fig. 3 which indicates, for various values of the visible and window channel, the cloudiness amount (opaque and non-opaque), the significant low cloud amount and the precipitation. Although the figure is based only on a very limited number of surface reports, it does show the potential of using a combination of window and visible data for cloud identification. In order to construct Fig. 3, it was necessary to perform smoothing. Several surface observations still appeared to be in substantial disagreement with the MRIR data; an actual surface report for one of these cases is indicated in Fig. 3. Inspection of the location of this observation (42° 55'N, 106° 28'W) indicated that it was within a small scattered cloud area at the edge of an extensive cloud sheet (see Fig. 1 or 2) and that the local state of the sky was changing rapidly. Either location errors in the MRIR data or unrepresentativeness of the surface reports could easily have produced the apparent discrepancy between the two sources of data.

3. Future Research Considerations

As previously mentioned, the channels with the most promising immediate operational use are the window channel and the visible channel. Channels 3 and 4 (Fig. 1) are mainly concerned with the heat balance of the earth and will find greatest application in research and in future

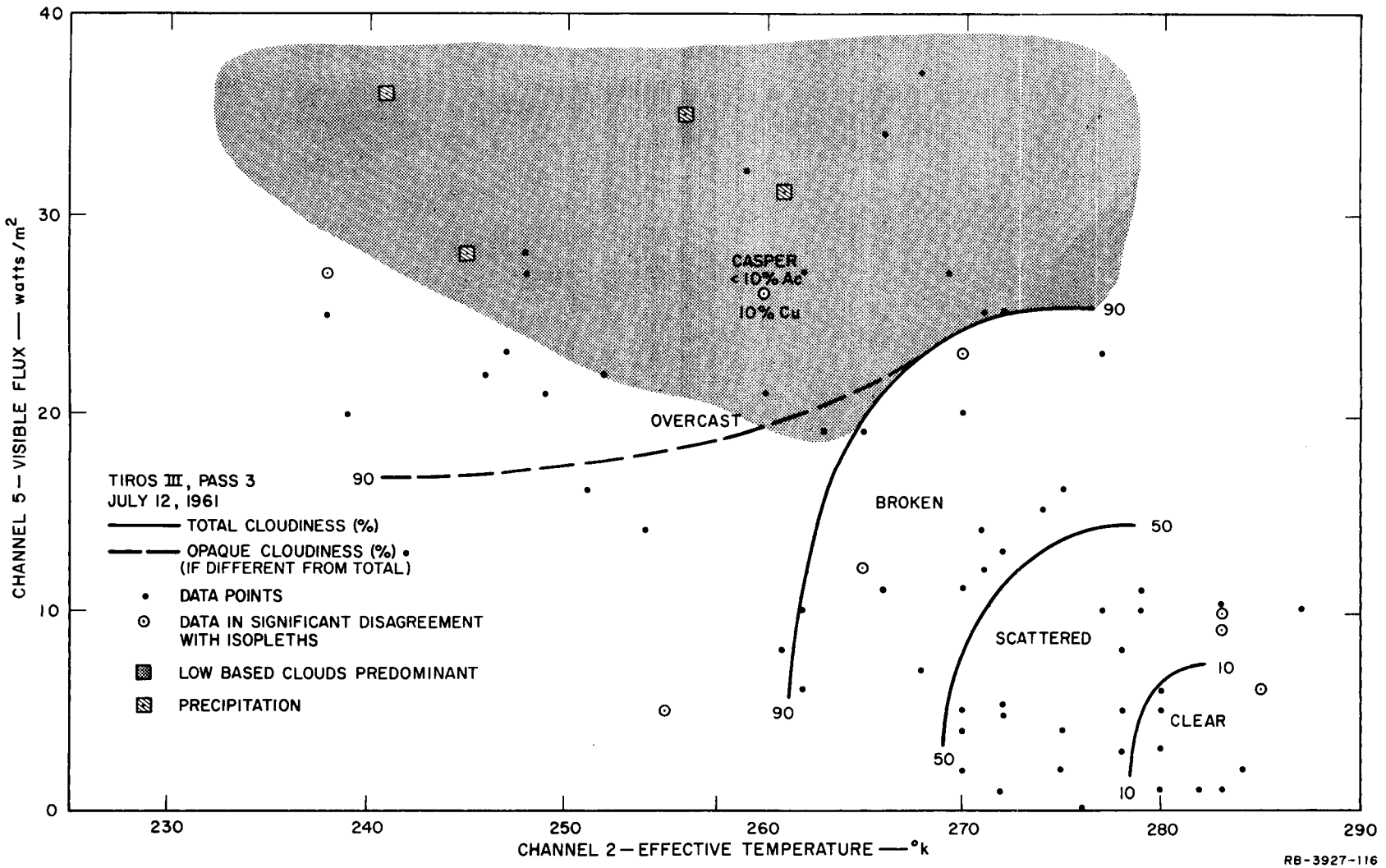

FIG. 3 MRIR Data (Channels 2 and 5) RELATED TO SURFACE CLOUD DISTRIBUTIONS FOR 12 JULY 1961 (MRIR Data, 1540-47Z; Surface Data, 1600Z)

numerical treatments of long range forecasting. The use of other spectral ranges has also been suggested (by Hanel[8] in 1961 and by Yamamoto and Wark[9] in 1962), but their appearances will depend on instrumentation research and development.

From this study, it has become very clear that continued meteorological research will increase the effectiveness of and confidence in the operational use of the MRIR data. The following areas of activity are suggested in connection with meteorological satellite MRIR measurements:

(1) Specific and statistical investigations pertaining to the effects of limb darkening, scattering angle, etc.

(2) Development of methods and automatic techniques for handling such conditions as partial cloud cover, snow cover, mountains, non-uniformity, etc.

(3) Quantitative verification programs which involve simultaneous aircraft, balloon, and surface measurements

(4) Studies of the relationships between various MRIR distributions and synoptic models.

Finally, while the above efforts would lead to better interpretation of MRIR data, it would be worthwhile to construct a climatological manual to serve as a provisional guide for the practical application of the data.

B. HRIR Data

The Nimbus satellite is also scheduled to carry a radiation sensing instrument of a high spatial resolution--8.6-milliradian field of view. This HRIR unit will therefore provide radiation data more comparable in detail to the AVCS than will the MRIR. The instrument will be operational during the dark half of the orbit and will measure emitted radiation in the 3.4- to 4.2-micron spectral interval. Assuming that there is negligible emission from the atmosphere itself (true between about 3.4 and 4.0 microns), its response should have similarities to the MRIR window channel (10.0 to 11.0 microns). A comparison of the energy flux that would be received by these two window channels can be estimated by referring to Table II, which assumes that the emitting surface is a

blackbody. As can be seen, in the HRIR region, considerably less energy is emitted than in the MRIR region. On the other hand, the HRIR window channel should sense more contrast between different surface temperatures.

Table II

ENERGY FLUX (LANGLEYS/MINUTE)
EMITTED BY BLACKBODY SURFACES OF SPECIFIED TEMPERATURES

Spectral Response	Temperature		
	200°K	250°K	300°K
3.4μ - 4.2μ	0.4×10^{-5}	16.7×10^{-5}	195.2×10^{-5}
10 μ - 11 μ	4.5×10^{-3}	17.6×10^{-3}	44.1×10^{-3}

The operational applications of the MRIR window data previously discussed may carry over to the HRIR data. Possibilities of converting HRIR data to both cloud top height and quantitative total cloud amounts were suggested by Blankenship[10] in 1962. Some of the assumptions made in converting MRIR window data to physical parameters may, however, not be as valid for the HRIR data. For example, the assumption that the emitting surface is a blackbody radiator may not prove as acceptable for the HRIR measurements as it has for the MRIR. Also, the HRIR window is not expected to be as clear as the Nimbus MRIR window. Although the region is essentially free of water vapor absorption, the HRIR spectral response will include some contribution from the strong CO^2 absorption band above 4 microns. Until it can be demonstrated that the HRIR can provide quantitative results, and that it is at least as satisfactory as the MRIR window data, there would appear to be little justification for a quantitative presentation of the HRIR data.

For the present operational systems, the HRIR response would serve its most useful purpose if presented as a continuous gray scale without attempting to measure its exact energy value. In this form, it should provide a general description of the nighttime cloud distribution and be an invaluable counterpart to the daytime AVCS. It is for this purpose that the HRIR instrumentation was originally intended. An HRIR gray scale would have some likeness to the one drawn for the TIROS MRIR Channel 2 effective temperatures (Fig. 4). In fact, it should appear identical to the eye except for showing greater detail. After a Nimbus vehicle has provided experimental data, it may prove feasible to convert the HRIR data into a quantitative form, either confined to selected small areas or in its entirety. If so, a modified version of the MRIR presentation (Sec. IV) could be applied to the HRIR.

FIG. 4 CONTINUOUS GRAY LEVEL PICTURE

IV FORMAT OF MRIR DATA

A. Basic Considerations

1. Magnification of Data

Since the MRIR viewing angle is 2.8°, and the satellite altitude is 500 nm, a resolution element covers an area 24 nm square at the SSP. The data obtained near the horizon are badly distorted and measured in small angles; therefore, only the center portion of the data--that observed within nadir angles less than 54.5 degrees--is of interest.* This corresponds to an earth distance of 1720 nautical miles and is more than sufficient to provide complete earth coverage at the equator. Each line will contain 39 elements between nadir angles of ±54.5 degrees, approximately 440 lines in half an orbit. The aspect ratio of the original data is thus about 11 to 1. A typical facsimile printer prints 100 lines per inch and 100 elements per inch along each line. If the MRIR data, in its unprocessed or raw form, were printed with such a printer, then one line of the MRIR scan would be represented by one printed line, and one MRIR resolution element would occupy one one-hundredth of an inch along the line. Each "printed" element could be one of several shades of gray, depending on the value of the corresponding data. Then the printed output will consist of a gray-level picture whose size is 0.39 inch by 4.40 inches.

Such an output is defined as a natural strip projection. It is the same projection used for the HRIR data. It is the most natural projection to use since each line of the output corresponds to a mirror scan line, and the distance along each output line is proportional to the mirror scan angle. No mathematical transformations are used to output the data.

It is obvious that a picture of this size is simply too small for operational use. It is proposed that the natural strip be magnified in

---

* Note Fig. 19, in Sec. VI.

both linear directions--the resulting output is denoted as a magnified-natural-strip projection. A good magnification factor is the value 20. The resulting picture would then be 7.8 inches by 88 inches. In this picture, each element of data would be repeated for a total of 20 picture elements along a line (before the next data element is printed). And each magnified line would be repeated for a total of 20 lines. Thus, each element of data is represented by a square that is 0.2 inch on each side. Other magnification factors can also be used with good results. A factor of 10 would result in a picture 3.9 inches by 44 inches. Each data element would then occupy a square 0.1 inch on each side.

Rectified and magnified outputs are also possible. For example, polar stereographic or Mercator projections can be used. Rectification would require considerably more data processing than the natural-strip format. The feasibility of rectifying MRIR data is considered in Section VI.

2. Information Required

As described in Section III, MRIR data are useful for two types of reasons: (1) the broad patterns of high and low IR values are of interest, and (2) the actual numerical values are of importance. This second requirement is in contrast to the AVCS and HRIR data, where only continuous gray-level pictures will be produced. Because it is quite difficult to read the absolute gray-level value of any desired point from a gray-level picture, some other information, such as superimposed contour lines (isopleths), must be added to the MRIR picture.

As in the AVCS and HRIR pictures, it is also necessary to identify the lines of latitude and longitude on the pictures. This can be accomplished by indicating the intersection points of selected grid lines.

B. Output Formats

There are several possible ways to produce an output that depicts both the high and low regions, and the actual values of the data. The following is a listing of possible formats. Each of these is

discussed and pictorial examples are given. Of these various formats, it is concluded that the shaded numerals are the best:

(1) Continuous gray picture
(2) Discrete gray picture
(3) Array of numbers
(4) Outline of numbers
(5) Contour lines
(6) Contour lines with additional information
(7) Numbers and gray level
(8) Shaded numerals.

The temperature range of the data collected from Channel 2 is 200°K to 320°K. For operational use it is believed of sufficient accuracy to indicate the temperature to the nearest 10°K. There are thus thirteen significant temperatures with the values 200, 210, 220,..., 310, and 320. The number of possible data levels is of importance in selecting acceptable output formats.

1. Continuous Gray Picture

In a continuous gray picture, each data element is printed to the most accurate shade of gray that exists in the output printer. For example, the temperature of 200°K would be produced at "pure" white (or the inverse, 200°K represented by black and 320°K by white). A temperature of 320°K would be "pure" black; and a temperature of 267°K would be produced at a gray level that corresponds to 67/120 = 55.8% black. The output picture would resemble a photograph, with the exception that each "grain" of the photograph would be 0.2 inch square. The number of different shades of gray possible in this picture, is restricted only by the characteristics of the printing device. (Either the darker, or the lighter, gray levels can represent the lower end of the temperature range. Both ways are referred to in this report.)

The advantage of this format is that the high and low regions are quickly and easily identified. The disadvantage is the difficulty of determining the exact gray level of any particular data element. The human eye is very sensitive to changes in gray level and to patterned

information, but poor at evaluating the absolute value of gray shades. The human observer tends to judge the gray level of any position relative to the shades of gray in the immediate vicinity. An example of this format is given in Fig. 4. The data used for this figure were obtained from Channel 2 of TIROS III, Pass 3; these source data are shown in Fig. 5. Figure 4 was drawn by hand; an actual output would not appear as smooth. It is concluded that this format is not suitable for numerical purposes.

2. Discrete Gray Picture

Rather than allowing a continuous gray level, one can allow the printer to use only a few specific levels of gray. If only thirteen levels of gray are allowed (each corresponding to one of the values 200, 210, 220, etc.), then the temperature of 267°K would appear the same value of gray as would be used for the temperature 270°K. In this way, a set of contour lines are suggested, since all temperatures from, say, 265°K to 274°K would appear at the same gray level. Regions of constant gray would thus be outlined.

Between 200°K and 320°K, there could be thirteen bands of gray, as follows: 200-204, 205-214, 215-224, ..., 295-304, 305-314, and 315-320. Unfortunately, as stated previously, thirteen levels of gray could not quickly and easily be distinguished by the human observer, and the regional boundaries might be distinguished only with difficulty, if at all.

In Fig. 6, an example of this format is given where only eight gray levels are used. The temperatures corresponding to the levels are also noted in this figure. Six of the levels correspond to changes of 10°K each. For the low temperatures, however, white is used to include the range 200°K to 230°K, and for the high temperatures, black is used to include the range 290°K to 320°K.

This figure was also produced by hand; that is, all shading was done by pencil as carefully as possible. The data used for this figure are also from Fig. 5. A similar output format is presented in an article by W. Nordberg. [11]

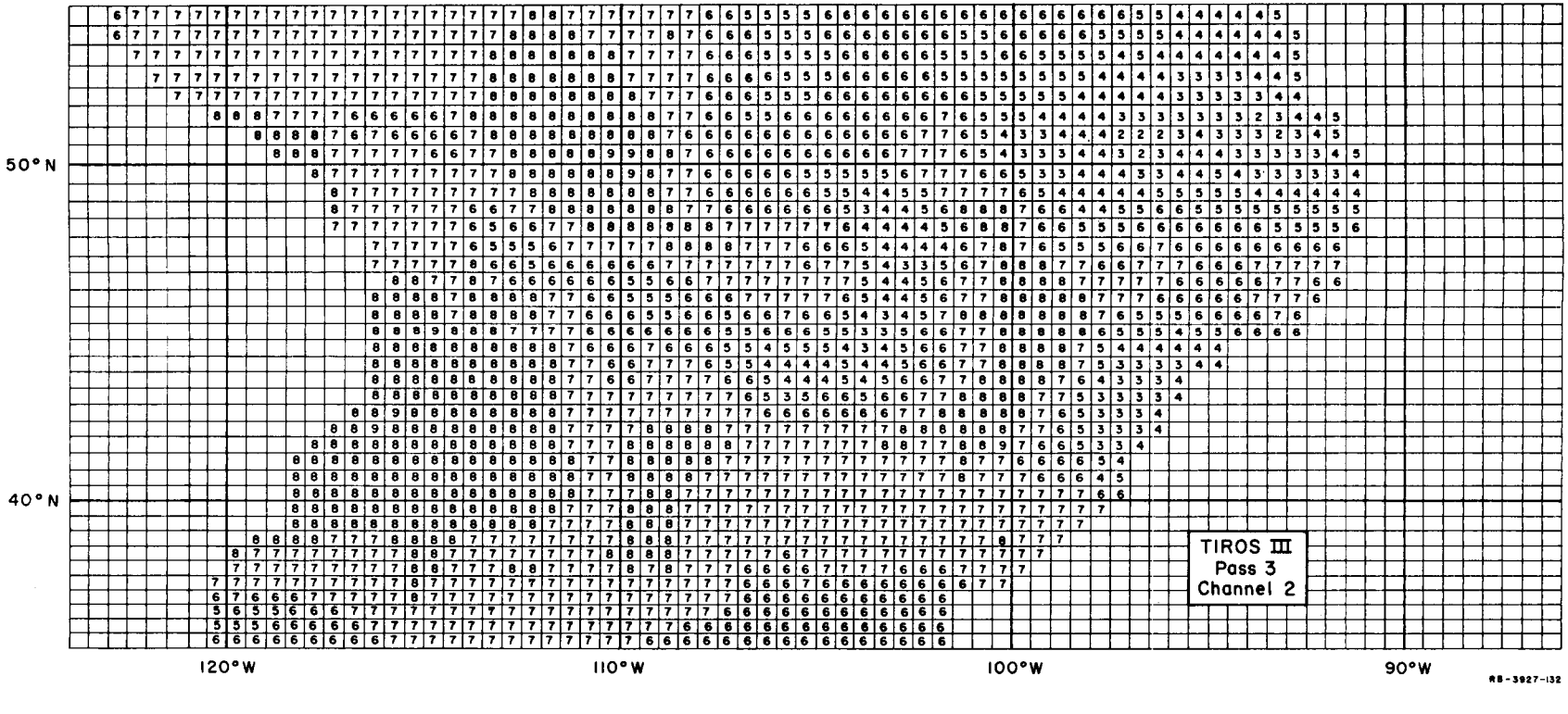

FIG. 5 ARRAY OF NUMBERS

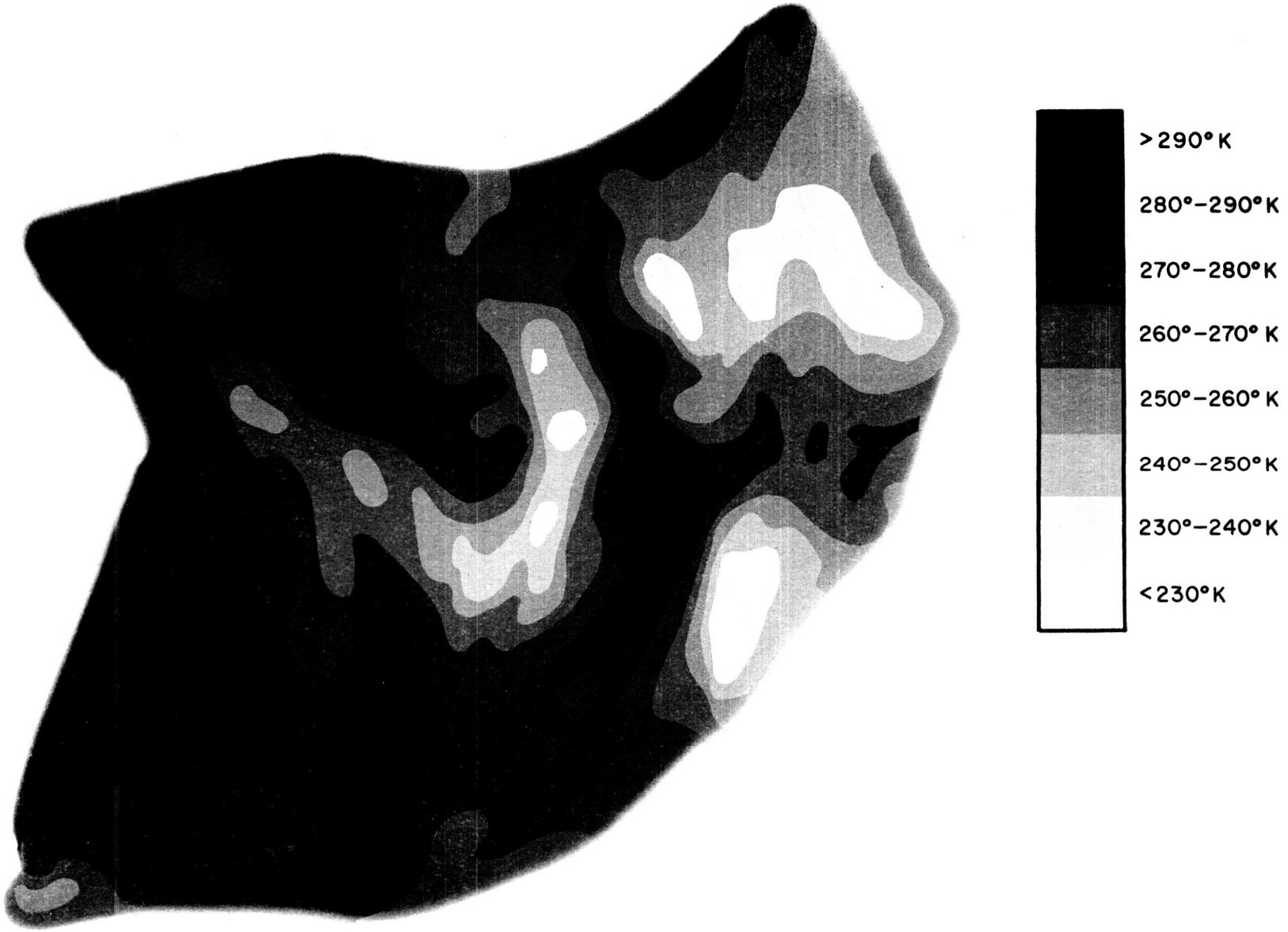

FIG. 6 DISCRETE GRAY LEVEL PICTURE

This format is easily read, both with respect to identifying the regions of extreme temperatures, and with respect to obtaining many of the actual numerical values. Its major disadvantage is that extremely low or extremely high temperatures cannot be numerically identified. The extreme values do not occur in the data used in Fig. 6, but this fact cannot be determined from the figure alone.

3. Array of Numbers

This format is simply a tabulation of data. The array for a complete half orbit could have 39 values per row and 440 rows. Each value would range from 200°K to 320°K. Figure 5 is an example of an array of numbers for a portion of an orbit. The latitude and longitude of the area is noted. The numbers have the following meaning: 2 represents 220°K, 3 represents 230°K, 4 represents 240°K, etc. The disadvantage of this format is the difficulty of visually determining the regions of similar temperatures.

4. Outline of Numbers

It is possible to selectively eliminate numbers from the full array of numbers presented in Fig. 5. One such method is to eliminate any number if each of the four numbers immediately surrounding it have the same value. The four numbers used are those to the right, to the left, directly above, and directly below. In Fig. 7 such a format is displayed. The regions of constant temperature are thus quickly outlined and fairly easily read. However, in large portions of the picture, where rapid changes exist, practically no numbers are eliminated and a full array remains. Additional data processing must be used to obtain this format, since comparisons between adjacent lines of data must be made in addition to comparisons along each individual line.

5. Contour Lines

In addition to gray level formats and numeric formats, a third basic format is to produce a set of appropriate contour lines (isopleths). Figure 8 is a copy of a typical surface pressure chart. This chart was produced by the Fleet Numerical Weather Facility, Monterey, California. A polar stereographic map of the northern hemisphere is preprinted on the

FIG. 7 OUTLINE OF NUMBERS

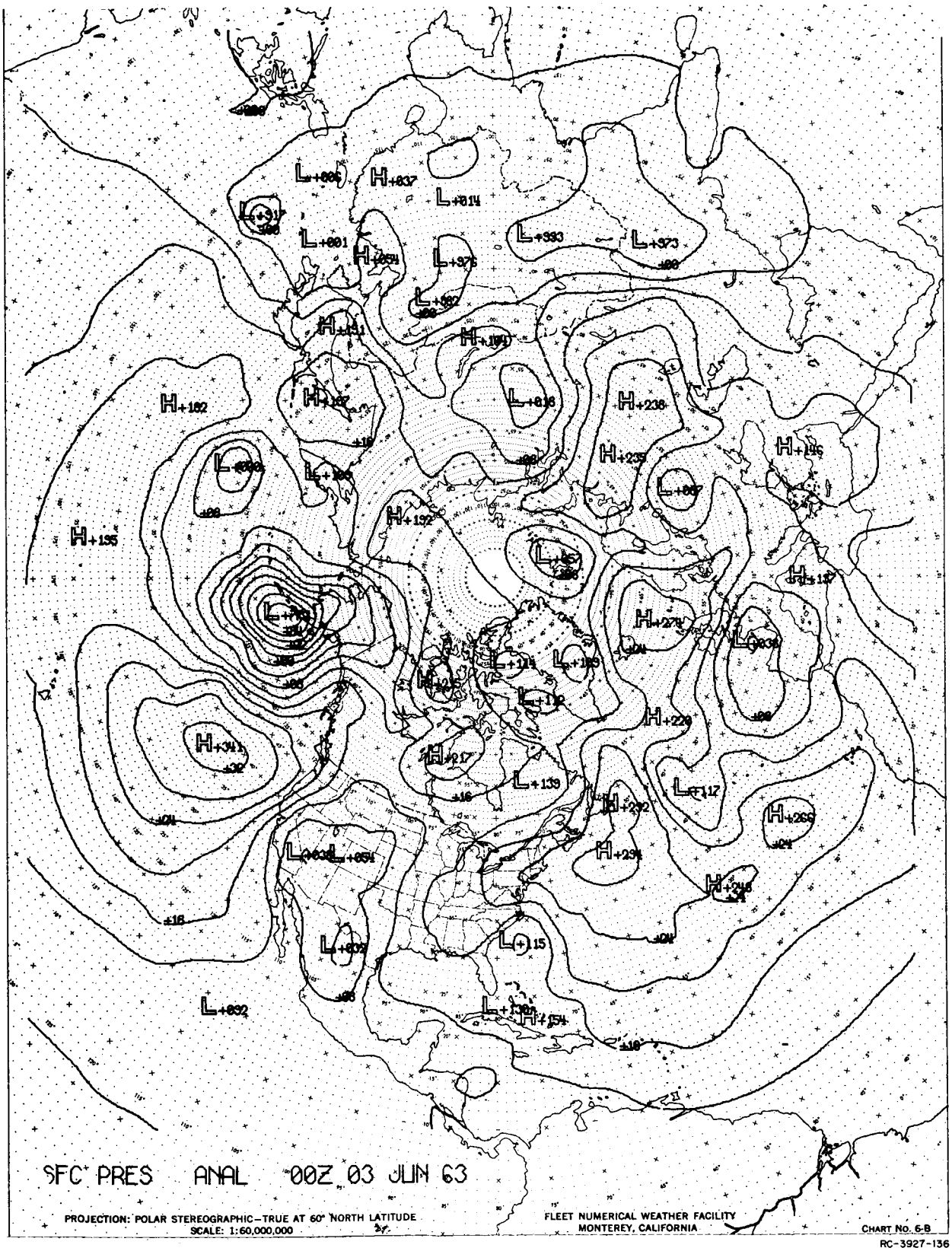

FIG. 8 NAVY CONTOUR MAP

plotter paper. Every other contour interval is identified by its value at the "bottom" edge of the contour line. In addition all absolute and local extremal values are indicated, where H is high and L is low.

In brief summary, this chart is produced as follows: Starting with an array of 63 by 63 data points (3,969 points), a CDC-1604 determines the location of all contour lines, and the extremal values, in about 2 minutes. The contouring algorithm that was developed at the Fleet Numerical Weather Facility is presented in Ref. 12. Using a Calcomp-565 line drawer, and a CDC-160A as a buffer store, Fig. 8 was produced in about 4 minutes.

Similar contour maps have been produced using an EAI (Electronic Associates Inc.) Series 3410 Dataplotter.

In Fig. 9, a hand-drawn contour chart is presented using the same data as in Fig. 5. The contour interval is 10°K; the lowest contour line is 230°K, and the highest is 290°K.

Such contour charts can be produced at each operational meteorological station using similar line-drawing equipment. Alternatively, the contours can be drawn at some central location and then re-scanned so that any facsimile printer can produce the chart. In either event, the contour lines must be actually drawn somewhere in the processing system. There is also a relatively large amount of data processing required, compared to other formats without contour lines. The largest objection to the use of contour lines is the difficulty of reading them. Except for the two prominent low and high regions in the left portion of Fig. 8, it is difficult to identify the low and high areas. Figure 9 is equally difficult to use. It is also a problem in many parts of the charts to quickly determine the numerical values of the data at specific positions.

6. Contour Lines with Additional Information

To make the simple set of contour lines more easily readable, one can add additional numbers or gray tones. A possible way of adding numbers would be to combine the contour lines with an outline of numbers. Figure 10 is a combination of Figs. 9 and 7.

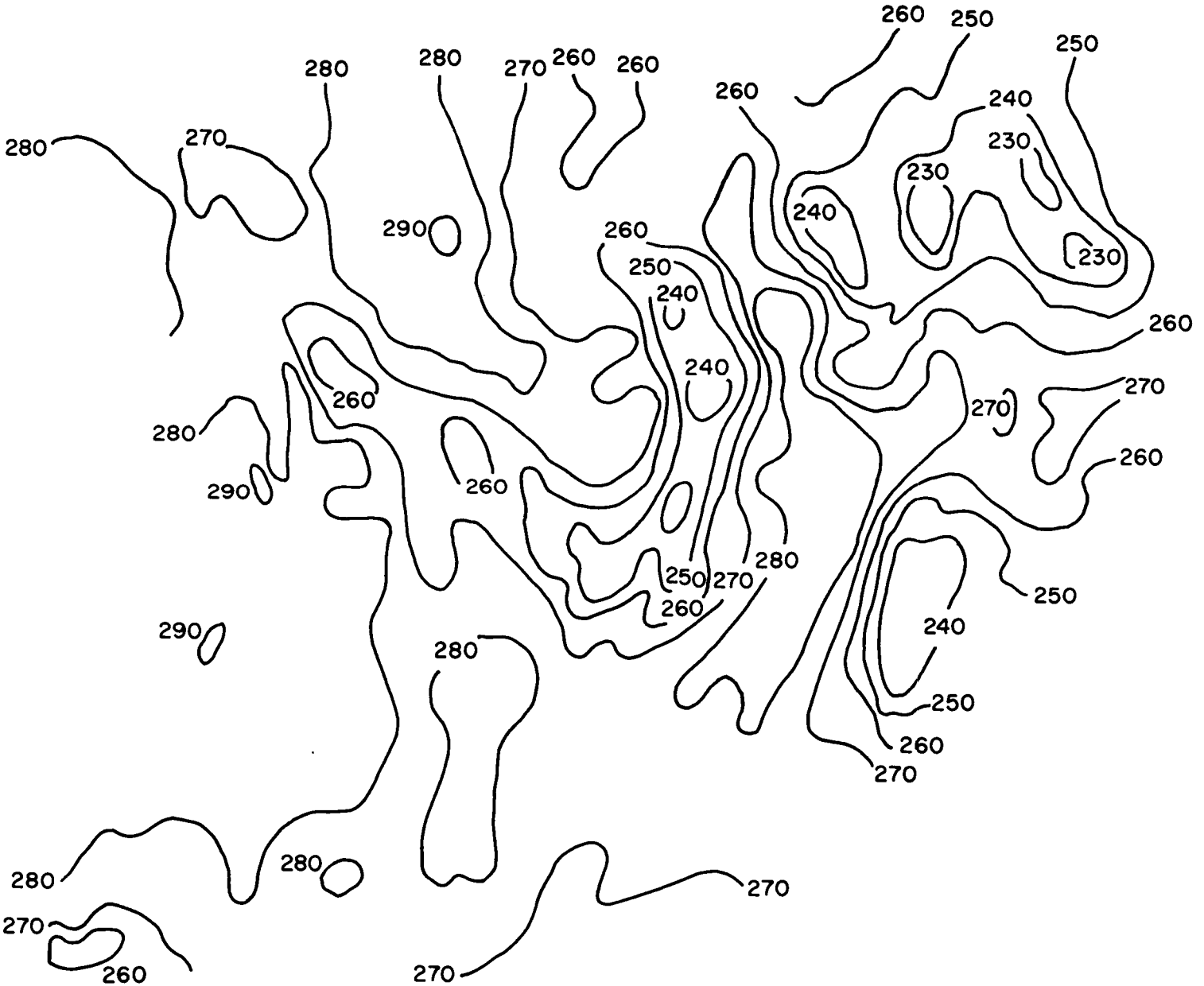

FIG. 9 CONTOUR MAP FOR TIROS DATA

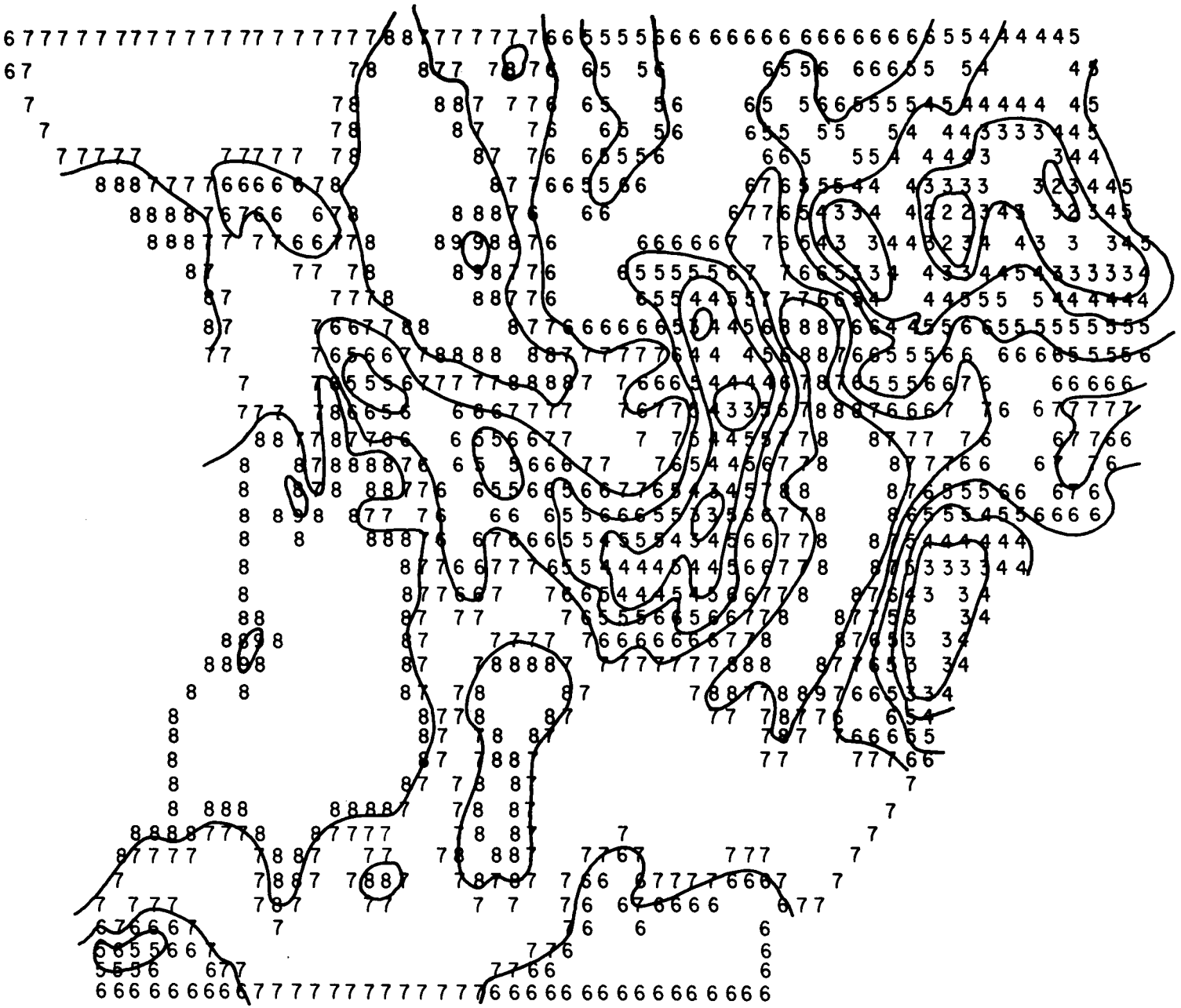

RB-3927-131

FIG. 10 COMBINATION OF CONTOURS AND OUTLINE OF NUMBERS

Addition of gray tones may be effected by combining the set of contour lines with a discrete gray level output. Figure 11 is a combination of Figs. 9 and 6. Figure 11 is an acceptable output format, but requires the same amount of data processing to generate the contour lines as in Fig. 9.

7. Numbers and Gray Level

Another combination of formats would be to superimpose an outline of numbers (Fig. 7) on a discrete gray picture (Fig. 6). The combined result is shown in Fig. 12. The resulting format is easily read and satisfies both objectives. The amount of equipment necessary to produce this format is similar to that required to produce Fig. 7.

8. Shaded Numerals

Some effort has been given to a particularly promising format where each of the numerals is somehow shaded. An example of the result that can be achieved is given in Fig. 13. The data on which this figure is based are given in Fig. 5, where a full array of numbers is presented. The format is also related to Fig. 5, but in Fig. 13, each number is presented on a varying gray-level background. Figure 13 is made at a scale of five data elements per inch. Figure 14 is similar to Fig. 13, except that it is made at a scale of ten data elements to the inch. (The left-hand edge of Fig. 13 is truncated for lack of space; the complete set of data is shown in Fig. 14.) As mentioned previously, there are a total of thirteen possible data values. The complete set of thirteen numerals is shown in Fig. 15. Figure 16 contains the actual gray values used to produce the two simulated output pictures.

The resulting formats (Fig. 13 or Fig. 14) allow one to easily distinguish the regions of high and low temperature. In addition, one can also easily identify the numeric value of each data point. The major advantage of this type of format is that a minimum of data processing is required. No interpolation is needed to calculate contour lines, and no comparisons between lines of data are needed to obtain an outline of numbers. Yet, the contour intervals are fairly easily identified. It is for these reasons that this type of format is particularly recommended.

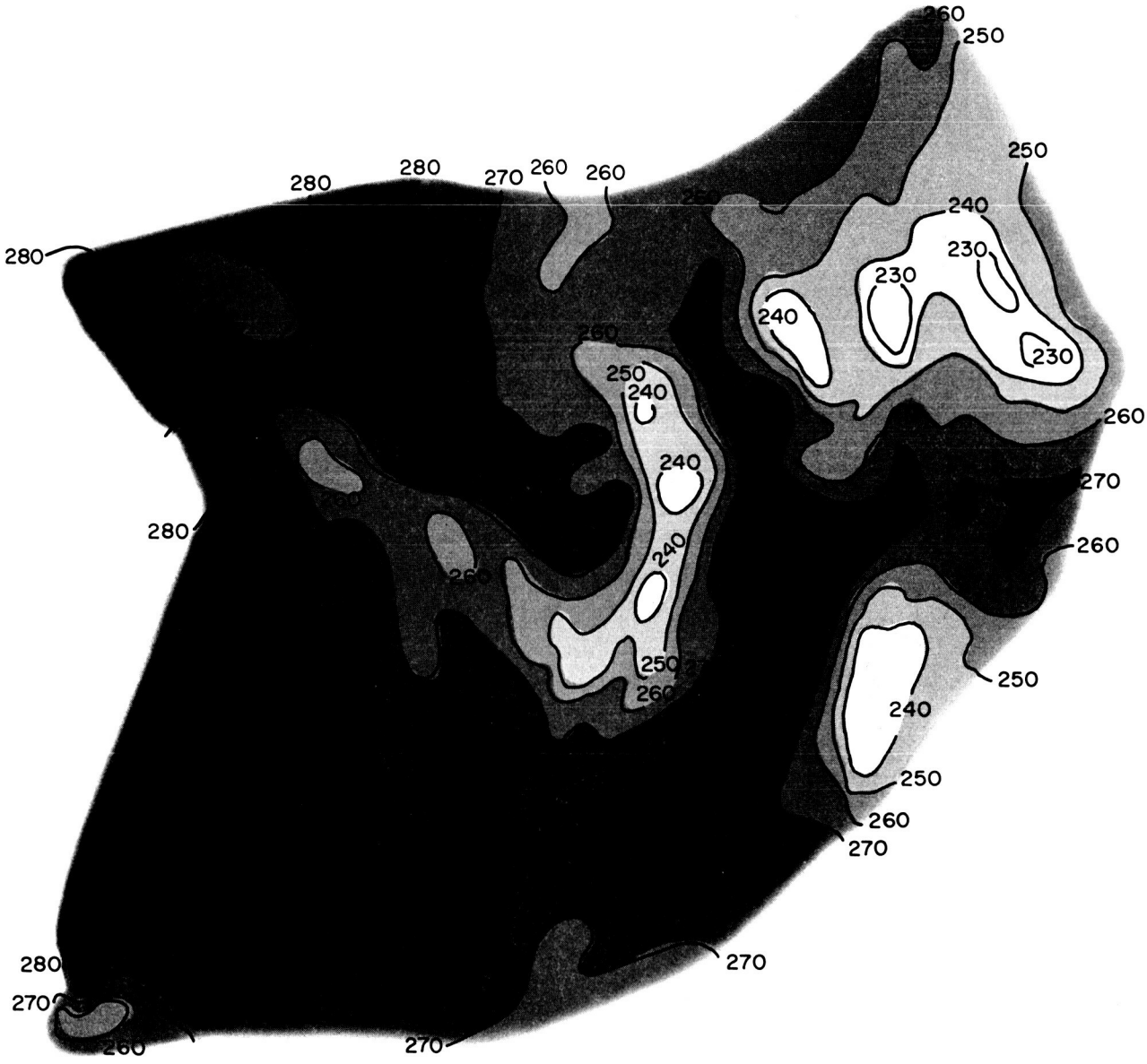

FIG. 11 COMBINATION OF CONTOURS AND DISCRETE GRAY LEVELS

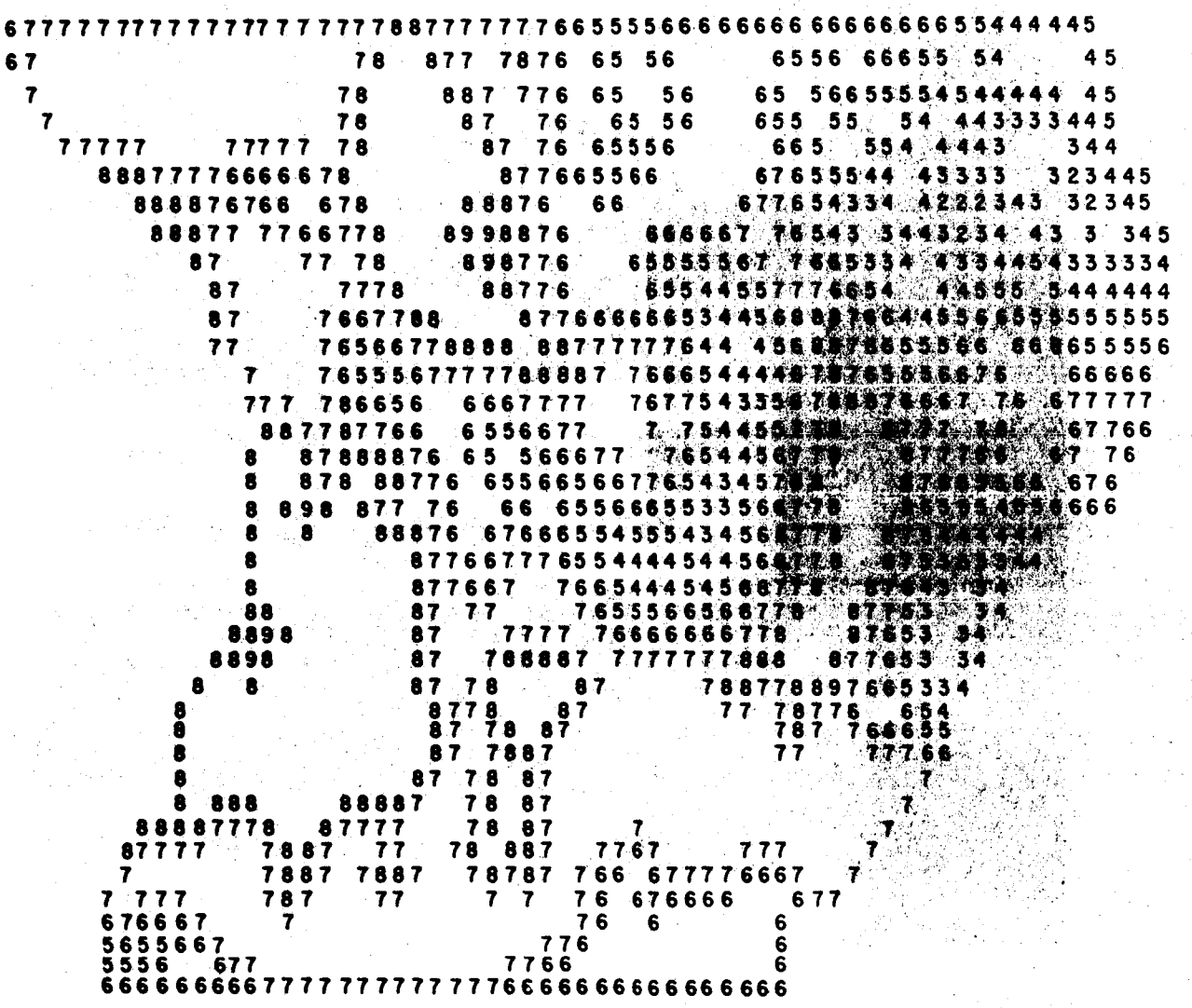

RB-9327-129

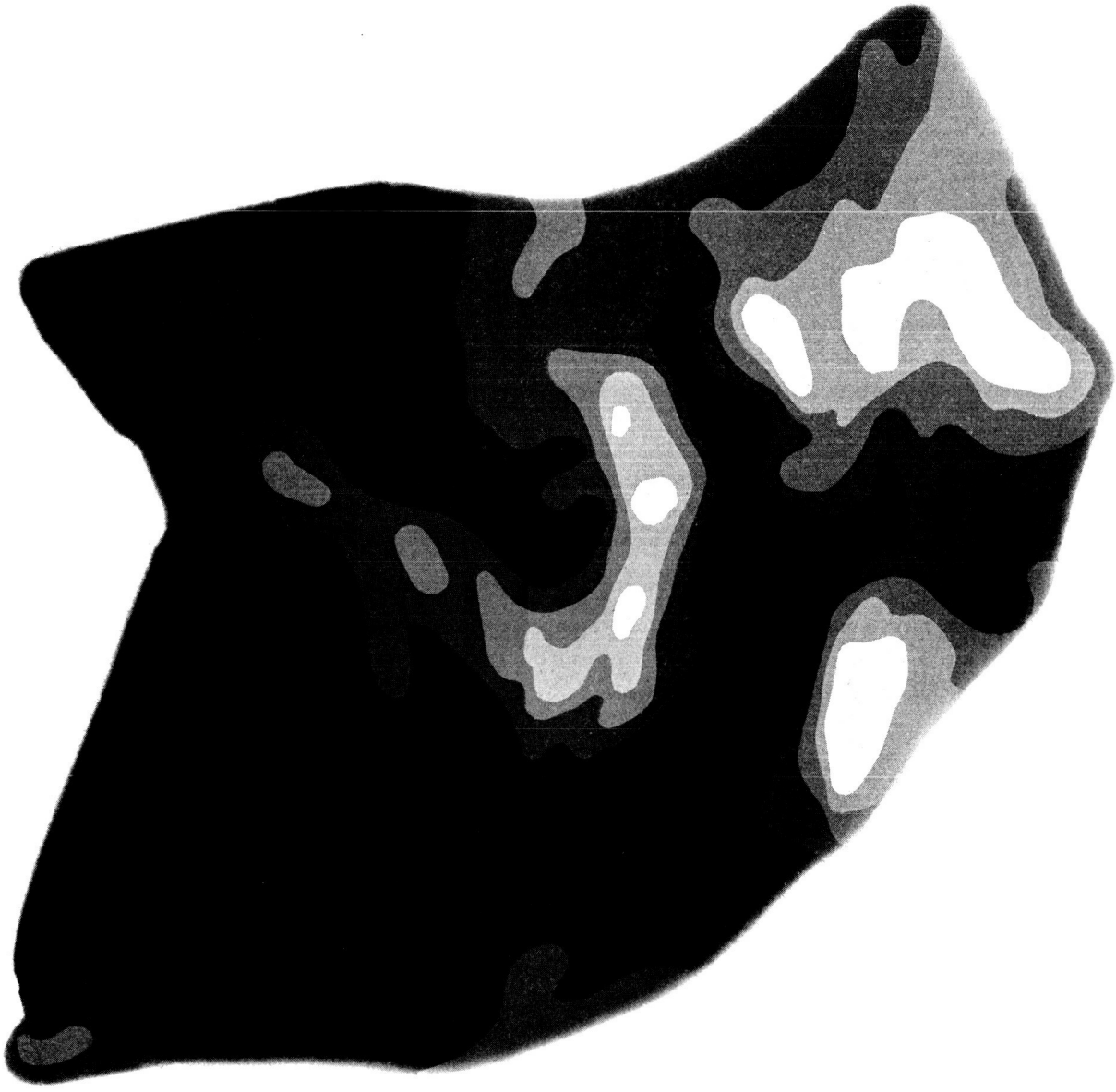

FIG. 12 COMBINATION OF OUTLINE OF NUMBERS AND DISCRETE GRAY LEVELS

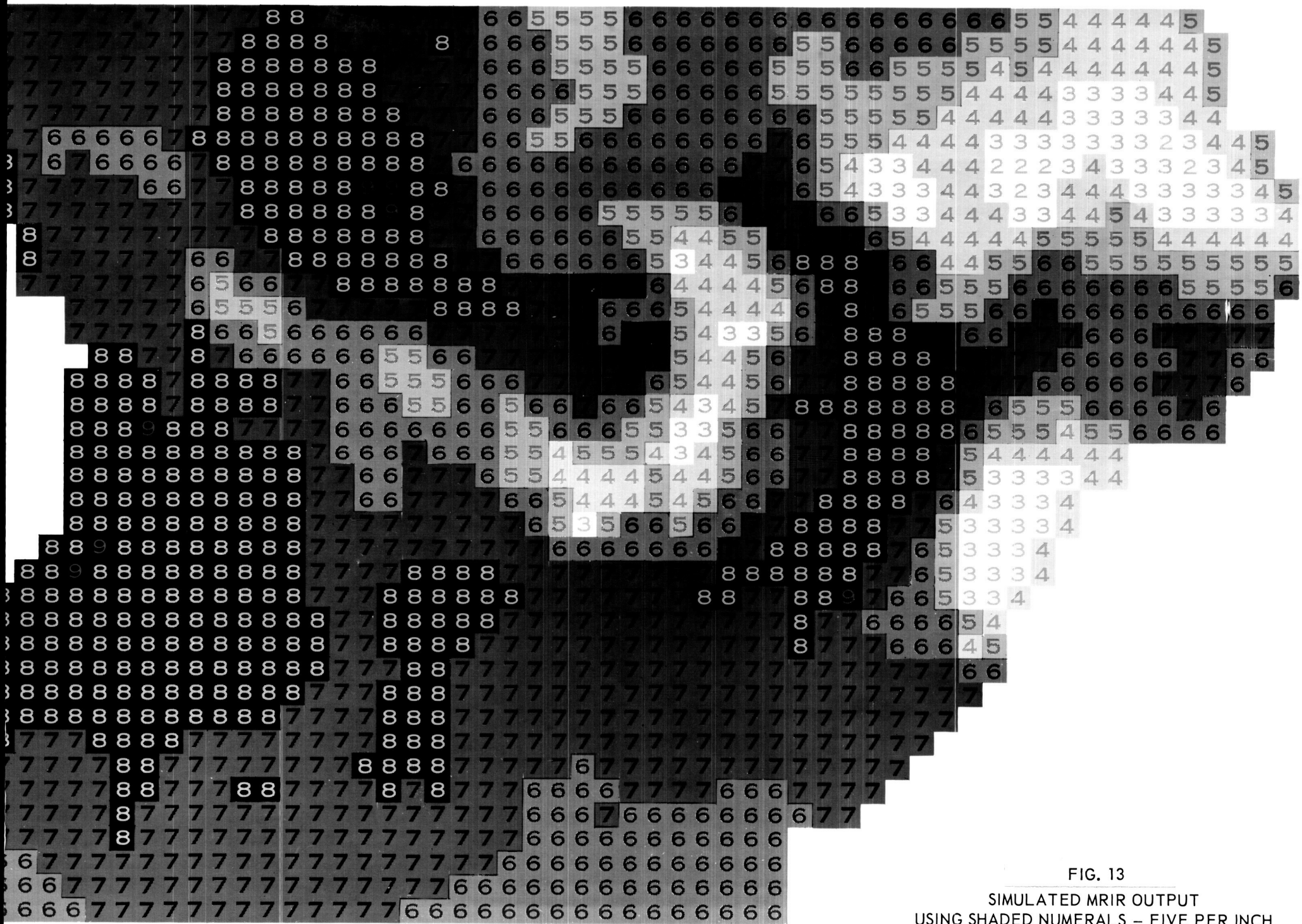

FIG. 13

SIMULATED MRIR OUTPUT
USING SHADED NUMERALS – FIVE PER INCH

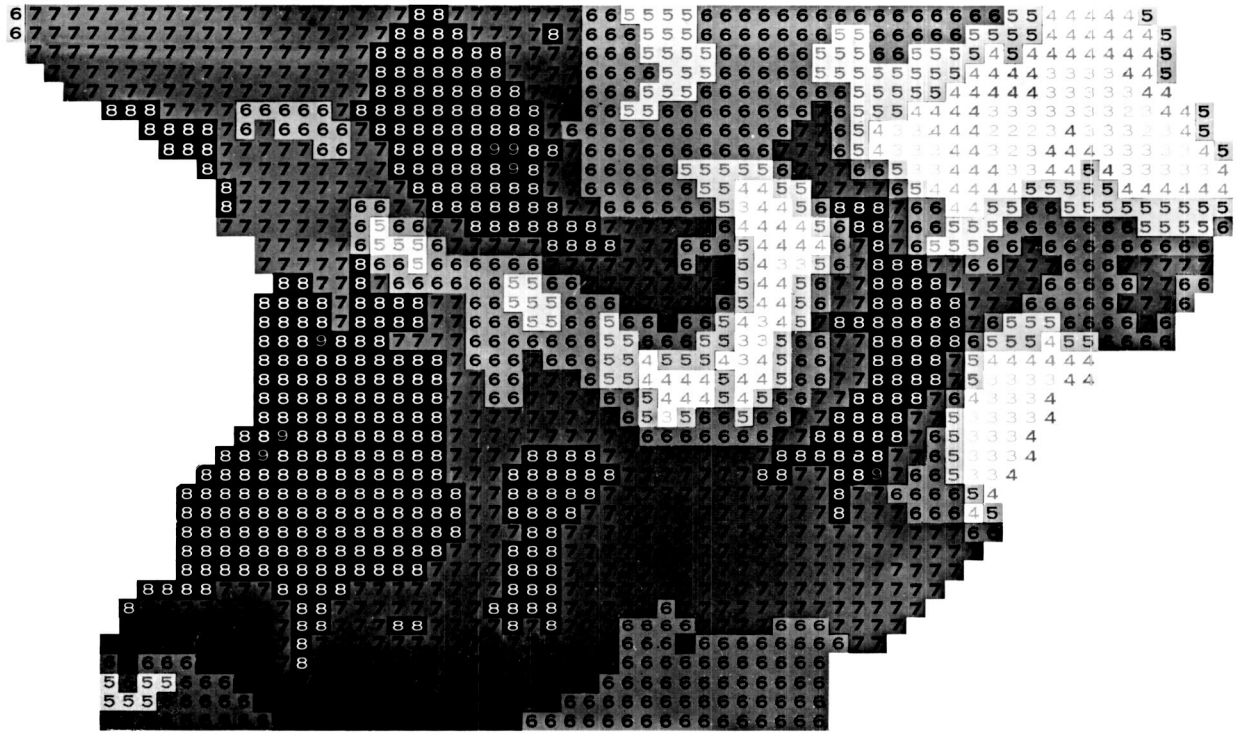

FIG. 14

SIMULATED MRIR OUTPUT USING SHADED NUMERALS – TEN PER INCH

FIG. 15

COMPLETE SET OF SHADED NUMERALS

TEMPERATURE, °K	NUMERAL	GREY LEVEL OF BACKGROUND	GREY LEVEL OF CHARACTER
200	0	WHITE (0%)	20%
210	1	WHITE (0%)	20%
220	2	WHITE (0%)	20%
230	3	WHITE (0%)	20%
240	4	10%	30%
250	5	20%	40%
260	6	30%	50%
270	7	45%	60%
280	8	65%	40%
290	9	BLACK (100%)	50%
300	0	BLACK (100%)	50%
310	1	BLACK (100%)	50%
320	2	BLACK (100%)	50%

RA-3927-133

FIG. 16 GRAY LEVEL VALUES OF SHADED NUMERALS

V MEDIUM RESOLUTION INFRARED (MRIR) DATA PROCESSING

By combining a number of standard state-of-the-art techniques, it is feasible to construct an electronic system capable of converting the MRIR video signals from recorded tape into a signal suitable for directly driving a facsimile printer. The output copy would be the shaded-numeral presentation described in Section IV-B-8, having grid points represented by a contrast in the gray scale.

A block diagram of such a system is shown in Fig. 17. The inputs to the system are a sampled digitized signal, 7 bits per sample, for the radiometer output, a pulse coincident with the start of MRIR data corresponding to the "view" of the earth, and a pulse coincident with the video at times when a grid mark is desired.

The outputs of the system are the analog facsimile signal and the line synchronization signal. Since this system is on-line in effect, the average output facsimile rate depends upon the input rate. The data rates shown in Fig. 17 represent those corresponding to a 50-line-per-second facsimile system, and require an input-tape rate corresponding to 2.5 scanning mirror revolutions per second. This, in turn, is 0.75 of the tape speed during acquisition of the data from the satellite; the total time required to process a complete orbit is approximately 4.8 minutes compared to the 3.6-minute acquisition time. Slower facsimile systems would require proportionately more time for tape playing.

The operation of the system is as follows: Upon receipt of the data-start signal, the data signal is converted into a number of five-bit words, each word representing one picture element sample. Between 30 and 50 samples are sufficient to define the data signal corresponding to the earth-scan portion of each mirror revolution. The data rates shown in Fig. 17 are based on 50 samples per scan. The data is quantized into twelve levels (requiring four binary bits), which represent the twelve 10-degree intervals between 200°K and 320°K. In addition, each sample may or may not be a grid point, so that a five-bit word is necessary to completely specify each sample.

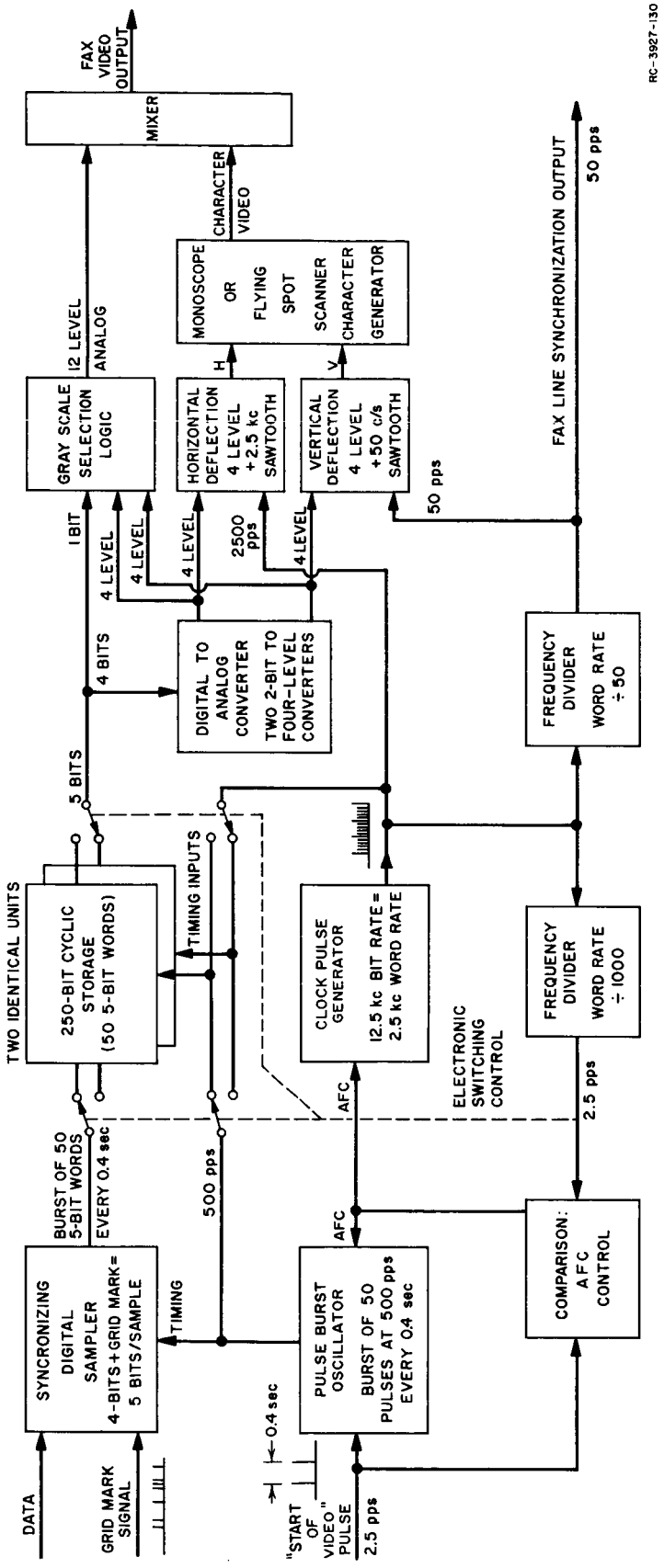

FIG. 17 BLOCK DIAGRAM OF MRIR DATA PROCESSING SYSTEM

The 50 five-bit words are stored in one of two identical cyclic memories, such as a shift register or magnetostrictive delay line, and subsequently read out twenty times. Sometime during the reading out of one of the cyclic memories, the other is loaded, so that on the completion of the twentieth read-out, the alternate memory may be switched in without delay. The read-out speed is compared with the tape recorder speed, and the frequency of the clock-pulse generator is so controlled that on the average the output and input data rates are equal. Since the read time required for the analog-to-digital conversion is less than (typically 25 percent of) the time required for the twenty cyclic read-outs, there is a fairly long waiting time between the A-D conversions so that there is wide tolerance in keeping the input and output rates equal.

The output of the cyclic storage, then, is a continuous stream of five-bit words. A block of 50 words repeats twenty times, followed immediately by a new block of twenty words repeating twenty times, and so on.

This continuous succession of words is converted to analog form in a D-A converter. For each word, a pair of voltages is derived, each having the possibility of occupying one of four values (levels). These time-varying voltage levels are used to determine the horizontal and vertical position of an electron beam in the CRT of a character generator, which may be either a monoscope tube or a flying spot scanner that scans a 35mm transparency. In addition to the initial positioning (by the D-A converter), the electron beam is deflected one character height (or width) by a pair of sawtooth waveforms. The frequency of the horizontal sawtooth is made equal to that of the word rate from cyclic storage, while the frequency of the vertical sawtooth is made equal to the new data rate, i.e., one-twentieth of the cyclic block rate.

Thus the video output of the character generator is a signal which represents the top horizontal slice of each of the required 50 numerals, then the next slice down of these same 50 numerals, and so on until the twentieth slice, representing the bottom slice of the 50 numerals, has

been completed. Then the signal continues with the top slices of a new set of 50 numerals, and so on.

In addition to the signal representing numerals generated in the monoscope (or flying spot scanner), a background gray-level signal is generated simultaneously in a circuit which combines the two analog deflection voltages in the proper four-to-one ratio. The resulting voltage level is normally mixed with the character video to supply the proper gray-level background. If, however, the grid-point bit is present in the word, then the voltage output is made to be white or black in accordance with whether the normal gray level would have been either darker or lighter than the middle value. In this manner, a contrasting rectangular area appears at the grid point locations.

The mixture of numeral video and background is a signal suitable for modulating a facsimile printer. Signal pulses for line return synchronization of the printer are obtained from the cyclic storage and occur at the end of each cycle of 50 words.

VI RECTIFICATION OF MRIR DATA

A. Introduction

Rectification of satellite data will result in a more useful presentation. Generally, the data would be rectified to a standard map projection--such as Mercator, or polar stereographic. Standard map projections are a more useful output since operational personnel are constantly working with such projections. A second advantage is that direct comparison can be made with other types of data presented on the same projection. Finally, rectification permits one to join adjacent pictures to form a mosaic of any given area of the earth.

Several previous studies[13,14] on the digital rectification of satellite weather data have shown that a significant amount of computer processing is necessary. In this report, a somewhat different approach to digital rectification is taken, and it is concluded that digital rectification of MRIR data is an attractive and feasible procedure. This conclusion is, of course, based on the amount of data generated by the MRIR equipment. For the AVCS pictures, digital rectification requires far too much computer processing so that a hybrid scheme has been recommended[14,15] for the AVCS problem.

In the following study the rectification process is first described in some detail. Included also are discussions of accuracy and uncertainties in the data. A brief summary is next presented of previous effort in this area. The new approach to digital rectification is then described. Three possible variations of this approach are studied in detail. One of them--called the gridded-tabular method--is recommended as the best way to produce rectified pictures. A brief flow chart of this method is given, as are timing estimates.

Future work in this area would involve the preparation of more detailed computer flow charts, and possibly the writing of computer programs for some of the sub-routines. More exact timing estimates can then also be made based on these results.

B. Digital Rectification--Some Background

Digital rectification can be described as follows. An initial picture, called the source picture, is given. It is desired to produce a final picture called the target picture. In this study, the final picture is assumed to be one of the standard map projections, such as Mercator, polar stereographic, conformal, etc. The source picture is produced from data collected at the satellite. Given the parameters of the satellite and the sensing device, one can (in principle) specify the mapping relationship between the source and target picture.

It is to be noted that neither the source nor target pictures are considered as analog pictures for the purposes of this study. The source picture is assumed to contain a number of discrete data elements, where each element corresponds to a resolution element in the sensing device. The value of an element is then simply the value measured by the sensor. These values can be displayed as numbers, or as gray levels (see Section IV). The target picture similarly contains a number of discrete elements. In either picture, the data elements are arranged in lines. The line spacing is equal to the width of an element, since each element is assumed to be square

1. Gaps and Overlaps

In general, a portion of the target picture can be either an expansion or compression of the source picture. For example, an area of 10 by 10 data elements in the source picture might map into an area of 13 by 13 elements in the target picture. Again, the same 10 by 10 source area might map into an area occupying only 8 by 8 elements in the target picture. These changes in scale result from the particular mapping function used, and also from the size of the desired final picture. In the expansion example, mapping each of the 100 source elements into the target picture will leave 169-100 = 69 unfilled target elements called gaps. In the compression example, the 100 source elements map into 64 target elements. There are thus 36 excess source elements that overlap other source elements when mapped into the target picture. Some of the 64 target elements will have only one source element mapped into them; other target elements will have two or more source elements.

It is necessary to fill in gaps in a rectified picture if the resultant picture is to be viewed by eye. Otherwise the absence of data simply distracts the viewer. One may fill an empty target element in two basic ways:

(1) Determine the closest non-empty target element, that has been mapped from a source element. Fill the empty element with the same value as this non-empty one.

(2) Locate a set of non-empty target elements, each of which has been mapped from source elements. Fill the empty element with, say, the average value of the set of values located.

When overlap occurs, the same two basic options are available:

(1) Select only one of the multiple values and use this as the value of the target element.

(2) Determine the average (or other function) of all the multiple values and use this average as the required value.

There are advantages for each possibility. In the first case, only the exact gray values that appear in the source picture can appear in the target picture. No new gray levels will occur. Thus a black and white checkerboard pattern in the source picture will also appear as a (distorted) checkerboard in the target picture. And the boundaries of the checks will be distinct. In the second case, the boundaries of the checks will be gray and will lead to fuzzy boundaries. However, all "ambiguous" picture elements are immediately identified by their gray tone. The averaging process tends to produce a somewhat smoother picture which may be easier to view. Perhaps the severest criticism of weighted averaging is that gradients in the source picture become less steep in the target picture. The exact location of a gradient may be in doubt (in the first case), but the gradient itself is better preserved.

As a final comment, it is observed that either gaps or overlaps can be completely eliminated in any target picture. One simply chooses an appropriate scaling factor. For example, to eliminate overlap, a scale factor is chosen such that there is at least a one-to-one correspondence in the region of minimum magnification from source to target. In a polar stereographic projection, for example, one would have one element at the pole correspond to one element in the source picture.

2. Gridding and Rectification Accuracies*

It is assumed that the rectified picture will also be gridded. While the two processes are closely related, there are some differences that deserve further discussion. The central topic is the accuracy required of each, since the accuracy in turn restrains the amount of approximation used (in either the gridding or rectification procedure). As a tentative conclusion, it is assumed that when a source element is rectified, its target position is accurate to within half a target element. Also as a tentative conclusion, it is assumed that a grid point will be computed to the same accuracy as the size of a source data element--namely, 24 nm. The principal factors entering into these conclusions are discussed below.

a. Location

One of the principal reasons for gridding the data is to locate the data with respect to the earth's surface. For example, it may be important to know whether the data are for land or for water. For some applications, it may be sufficient to locate the data within, say, 100 miles. In this case, the required gridding accuracy is much less than the resolution of the data (which is 24 miles at the SSP). For other applications, it may be necessary to locate the data to, say, 1 mile. In this case, the grid points must be located much more accurately than the resolution of the data. Specific examples of these two extremes can be given. It is sufficient to state, however, that gridding accuracy does not necessarily depend on the resolution of the

---

* In this discussion, accuracy of gridding refers to the accuracy of the gridding and rectification computations. Other sources of error exist, some of which are the following:

(1) Uncertainties in the satellite position.
(2) Uncertainties in the satellite attitude.
(3) Unknown position of the radiation source due to the coarse resolution of the sensor.
(4) Errors caused by the varying and unknown height of the radiating surface. A positional error occurs when, at nadir angles other than zero, it is assumed that the radiation surface is at the earth's surface and actually it is much higher.

data. To obtain the requirements for gridding accuracy, one must examine the projected uses of the MRIR data. As an initial estimate, it is assumed that the grid points will be located to the same accuracy as the source data.

One alternative to gridding the data is to rectify them to a standard projection such as polar stereographic. The location of only one point need be determined. The location of every other point is then known, and can be easily located using, for example, a transparent overlay that has grid lines printed on it. Thus, a suitably rectified picture is an equivalent to a gridded picture. (One can do both, by printing the grid points in the rectified picture and obviate the need for any overlay.) It is thus seen that the requirements for rectification accuracy are closely related to those for gridding.

b. Comparison

Another principal reason for gridding is to be able to compare the MRIR picture with other types of pictures--such as AVCS. These comparisons can be made side by side,or perhaps by using some type of transparent overlay. It might appear that the grid points for the MRIR picture should be determined to the same accuracy as the pictures compared with. (The AVCS grid points are determined to 0.4 nm.) However, since the inherent inaccuracy and coarse resolution of the MRIR data would make precise comparison impossible, the accuracy required should be based on the least accurate data, the MRIR.

c. Distortion

A secondary reason for gridding is to indicate distortions in the "shape" of the data if the rectification is not accomplished with high precision. Such distortions arise from attitude (yaw, pitch, and roll) oscillations. Each of the three attitudes has a maximum error of ±2°, and a maximum rate of change of 0.05° per second. These oscillations in the satellite cause a "wobble" to be introduced into the shape of the data. For example, suppose that a thin straight cloud was oriented north-south. An oscillation in the roll would cause this cloud shape to have a "wobble" of the same frequency as the roll frequency. As another

example, circular areas in the sky can be pictured as ellipses due to attitude oscillations. In some cases it is of importance to ascertain the true shape of the meteorological phenomenon. One way to indicate possible distortions is to completely grid the source picture. If, upon visual examination, the grid lines are not smooth curves then this indicates that oscillation was present. Another way to treat this problem is to rectify the source picture, using the known attitude errors in the rectification formulas. In this way all "wobbles" will be automatically eliminated, and all grid lines will appear smooth.

In the MRIR system, the resolution element is 2.8° wide. Thus the maximum attitude error is less than one resolution element. If the grid points are plotted to the same accuracy as a resolution element, then any wobble will not even be visually apparent. If the grid points are plotted to a finer accuracy, then any wobble will become evident. Since it has been assumed that grid points will not be determined to a better accuracy than a resolution element, it is concluded that shape distortions caused by attitude oscillation are not significant.

C. Summary of Other Efforts at Digital Rectification

There have been two known efforts at rectifying photographs taken from a satellite (TIROS TV pictures of cloud cover). The essential procedure of each effort is as follows: Starting with the resultant analog picture, a digitized source picture is prepared. The mapping relationship between the source picture and the target picture (map) is determined. Then each data element in the source picture is located into the target picture, using the mapping function.

In Reference 13, some saving is made in the number of data elements actually transferred by using a redundancy reduction technique. In this technique, each line in the source picture is examined; and all adjacent data elements with the same gray level are collected. Only the coordinates of the first and last element in such a linear group are then actually mapped. All intermediate elements are then simply entered--by linear interpolation--into the target picture between the two mapped elements. As a result of curvature in the Mercator projection used, the

two mapped elements cannot be more than 16 elements apart--otherwise linear interpolation is too inaccurate. A typical source picture contains 300 elements in each of 300 lines, resulting in 90,000 elements. Of these, approximately 22,000 to 32,000 points remain to be mapped after using the reduction technique. This net number of data elements requires about 12 minutes on an IBM 704. The same problem on an IBM 7090 is estimated to take 12/5 = 2.4 minutes.

In Ref. 13, it appears that the scaling factor is such that no overlap occurs. Gaps do occur and are filled as follows: Each empty target element acquires the same gray level as the closest non-empty target element on its left-hand side (on the same line in the target picture).

In Ref. 14, an IBM 7090 is used for rectification, and five mapping functions are available: polar and oblique stereographic, equatorial and oblique Mercator, and oblique cylindrical equal-area. Source pictures are digitized to contain both 240 by 240 elements, and 120 by 120 elements. No computing times are given, and no information is available on how the gaps in the target pictures are filled.

Both references contain photographic examples of the rectification process.

D. A Proposed Approach to Rectification

The following approach is an "inverse" of the rectification schemes investigated in Refs. 13 and 14, and appears to have several advantages. In this approach one goes from the target picture to the source picture, in the following manner:

There are several coordinate systems involved. The first is the u, v scan system of the source picture. The variable u is the line number, and v is an element within a line. Each variable is an integer and begins with the value 1. The second coordinate system is the w, z scan system of the target picture, where w and z are similarly defined. The third coordinate system is the set of natural latitude, ϕ, and longitude, λ, lines on the earth's surface. These coordinates are generally desired on

the rectified target picture, and it is assumed that they will appear on the final picture.

The first step in the proposed approach is to determine the latitude and longitude of each element in the target picture. A specific projection must be specified--for example, the polar stereographic. The latitude and longitude of each element $\underline{w}$, $\underline{z}$ is determined. These calculations need be performed only once, and can then be used over again as required.

The second step is to grid the source picture. Gridding methods to perform this task accurately and quickly have been developed. Once this picture is gridded, the latitude and longitude of any source element can be obtained, as needed, by simple interpolation.

The third step is to map the source picture into the target picture as follows: For each target element $\underline{w}$, $\underline{z}$, determine whether its latitude and longitude are within the source picture. If yes, then locate the source element $\underline{u}$, $\underline{v}$ whose latitude and longitude is the closest to the desired latitude and longitude position. The value of the source element so chosen is then stored in the desired target element. Continuing in this manner, all the target elements are filled.

The advantage of the above "inverse" approach is that overlaps and gaps are automatically taken care of, with no extra processing needed. When overlap occurs in a "direct" rectification scheme, one would have to select among the various values. In an "inverse" approach, the closest $\underline{u}$, $\underline{v}$ element is chosen and the others ignored. (For the MRIR data, it is anticipated that scale factors will be chosen so that no overlap will occur in any rectified picture.) When a gap occurs in a "direct" rectification scheme, one would select, using some extra processing, the nearest non-empty element on the same line. With even more extra processing the nearest non-empty element could be selected considering other lines as well. In the proposed "inverse" approach, the nearest non-empty element is automatically chosen, with no additional processing required.

To further study the "inverse" approach, three specific rectification methods are presented. Each is an "inverse" type of method, and they are

called the exact, the tabular, and the gridded-tabular methods. Each is described in some detail and the various advantages of each are stated. To carry out these descriptions a polar stereographic projection is assumed. The earth's surface can be completely mapped by two such projections--each terminating at the equator. Also, the linear scale at the equator is only twice that at a pole. Finally, this projection is commonly used for many purposes. Other projections are not ruled out. However, the purpose here is not to recommend a particular projection, but rather to investigate the feasibility of rectifying by digital methods. To this end, the polar stereographic projection is chosen simply as a good example.

E. Description of the Rectified MRIR Data

Before describing the three specific rectification methods, it is necessary to present the polar stereographic projection. It is also pertinent to summarize the MRIR scanning system and to indicate how these data appear on a polar stereographic map.

From among the five MRIR channels, Channel 2 appears to be the most immediately useful for operational purposes. The Nimbus satellite will travel in a noon-midnight orbit. It is proposed that all data collected on the "noon" side be presented on a different output than the "midnight" data. The original Channel 2 is thus thought of as two channels (Channel 2N and Channel 2M, with Channel 2N operating only at noon, and 2M operating only at midnight). In 24 hours, Channel 2N will view the entire earth's surface; in the same 24 hours, Channel 2M will also view the entire earth's surface. If one were to prepare a 24-hour mosaic for each channel, then four polar stereographic maps would result--a north and south polar stereographic map for each channel. For one complete orbit then, four rectified outputs are produced. Each such output ranges from the equator to one of the poles. (If the data to be measured were independent of the time of their collection, then only two polar stereographic mosaics would need to be made. Each such mosaic would be completed in 12 hours.) In any event, it is assumed that each complete orbit is divided into four quarter-orbits, where a quarter-orbit extends

from the equator to a pole. Attention will thus be focused on the rectification of a quarter-orbit.

The polar stereographic projection is commonly used for many weather applications, and a brief description of it can be found in Ref. 15. Figure 18 contains a portion of a polar stereographic map that ends at the equator. (The source map is a base map used for weather data purposes.) The scale change with latitude is shown at the bottom of Fig. 18, and is also described in Ref. 15. The linear scale at the equator is twice the scale at the pole; thus the area magnification is four to one.

1. The MRIR Gridded Area

Figure 19 displays the position of the satellite. As in the HRIR system, it is assumed that only the data within the central 109° will be gridded; this is also the area that will be rectified.

In order to determine the location of this swath on the earth, it is assumed that the earth is spherical, that the satellite's altitude is constant, that the three attitude errors (roll, yaw, and pitch) are each zero, and that the satellite has no forward motion during the viewing of each line. The effect of these assumptions (for the purpose of this discussion) is either zero or near zero. The reasons for this statement are given later.

In Fig. 20, the great circle WOE is the equator, the great circle NOS is a meridian of longitude, and the great circle AOB is the SSP track which makes an angle of 10° with NOS at the equator crossing point, O. The spherical triangle NOC_0 is the first triangle solved. Arc NO is 90°, angle NOC_0 is 10°, and the arc OC_0 is given various values from 0° to 90°. One then solves for the arc NC_0. Arc C_0D is then equal to (90° - NC_0) and is the latitude of the subsatellite point C_0. Angle ONC_0 is then obtained; it is the longitude of point C_0 with respect to point O.

The spherical triangle C_1NC_0 is the next one to be solved. Arc $C_1C_0C_2$ is perpendicular to the SSP track, since $C_1C_0C_2$ is the scan line through point C_0. One can thus obtain angle NC_0C_1. Arc C_1C_0 is 14.3°,

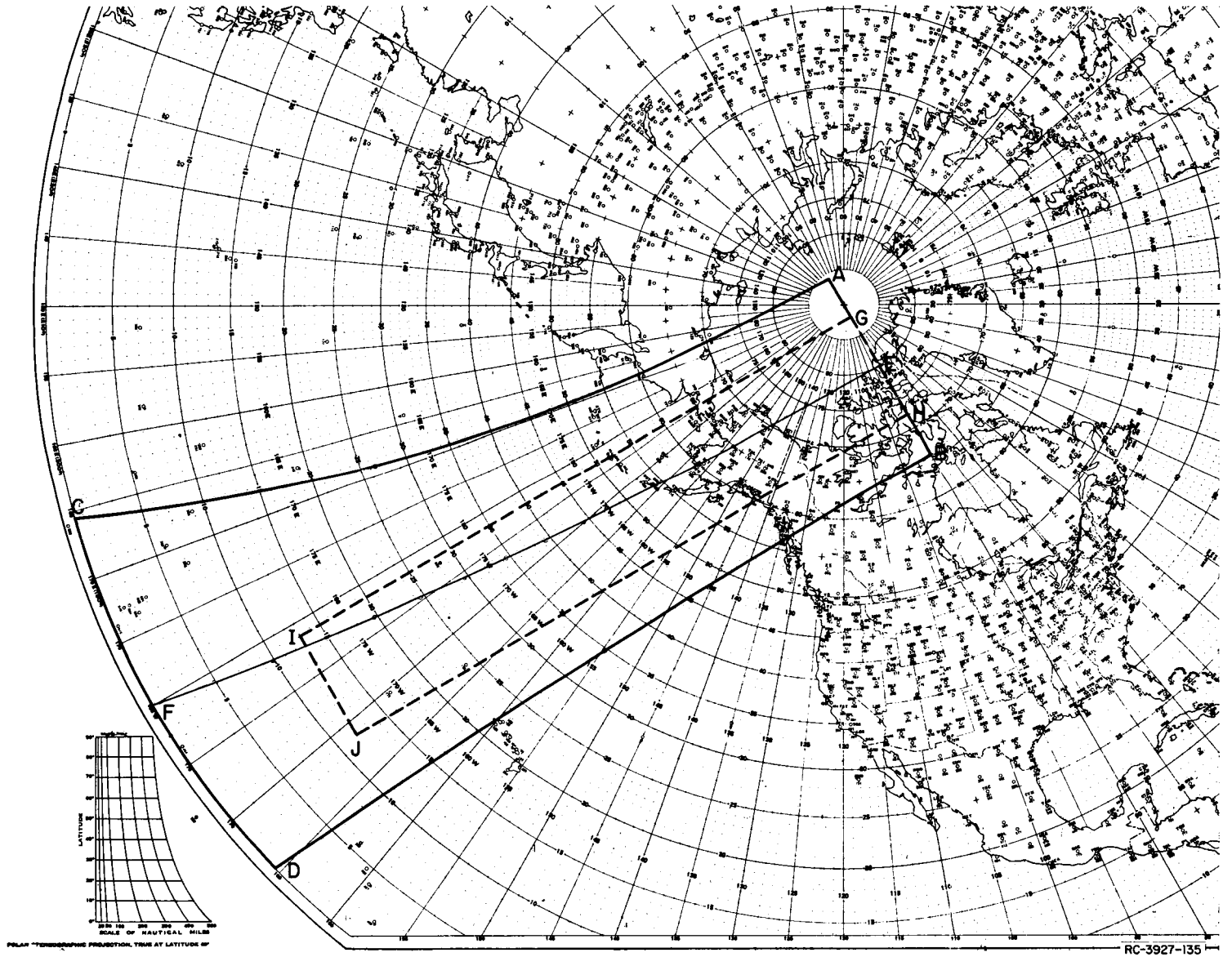

FIG. 18 POLAR STEREOGRAPHIC MAP SHOWING RECTIFIED AND UNRECTIFIED QUARTER-ORBIT

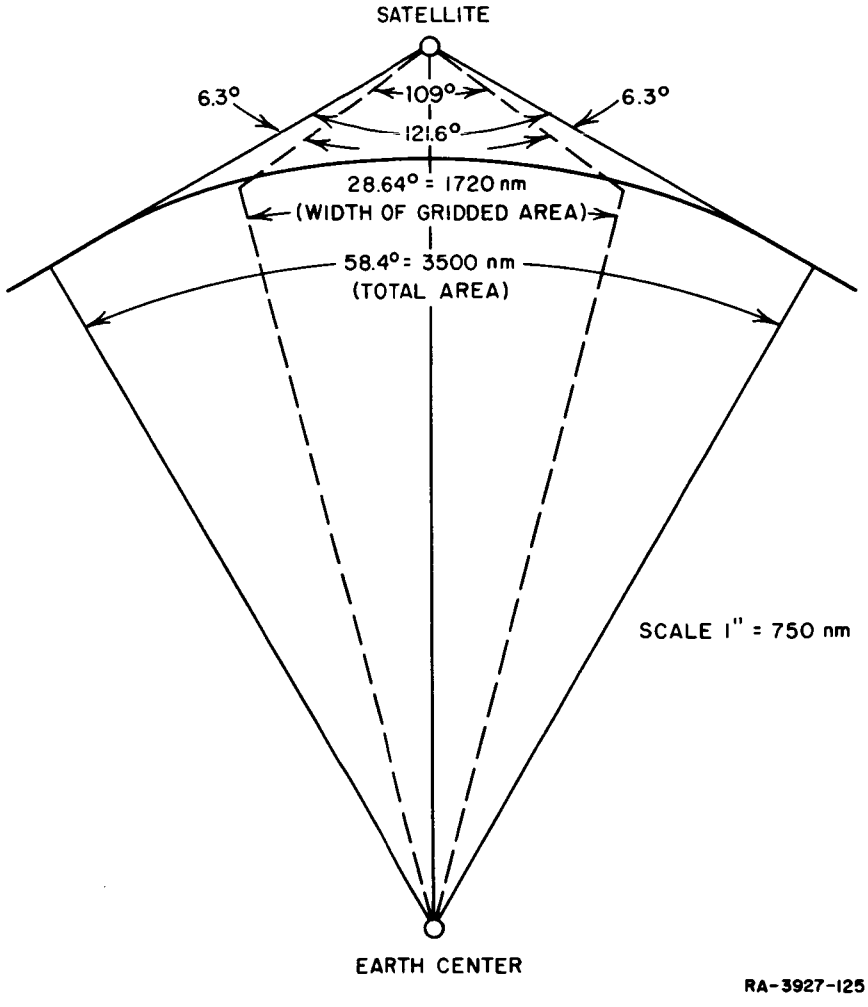

FIG. 19 SATELLITE POSITION ABOVE THE EARTH

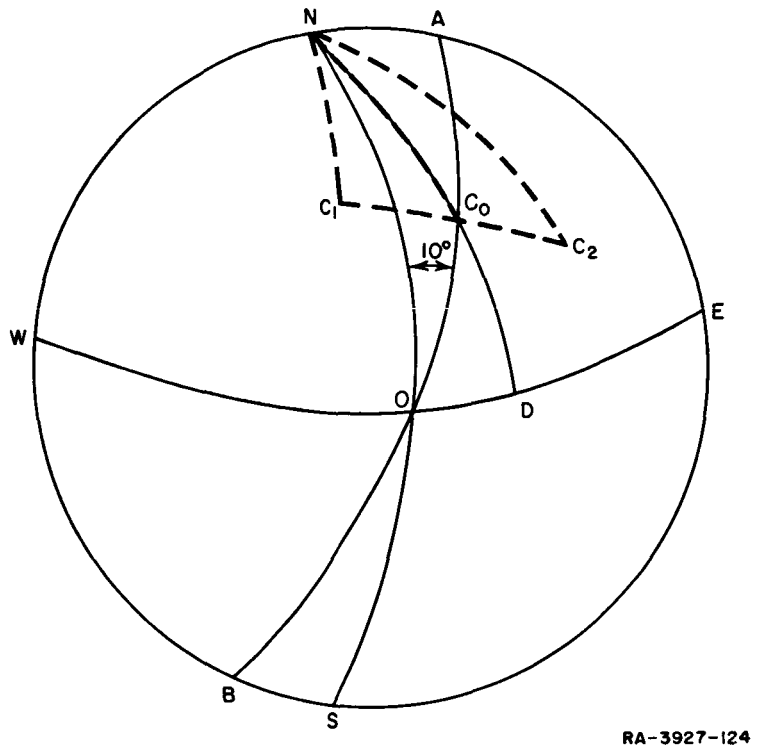

FIG. 20 THE SSP TRACK AND THE EDGE OF THE SWATH

which is the edge of the gridded swath (see Fig. 19). Knowing arc NC_0, from the previous triangle, one can then obtain arc NC_1 and angle C_1NC_0. These are in turn used to obtain the latitude and longitude of point C_1. In a similar fashion, triangle C_2NC_0 is solved to obtain the latitude and longitude of point C_2. Arc C_0C_2 is also equal to 14.3°.

In Fig. 18, the arc FE is the SSP track (and corresponds to the point C_0 as OC_0 varies from 0° to 90°). Arc CA, in Fig. 18, similarly corresponds to point C_1; and arc DB similarly corresponds to point C_2. The region ABDC is a polar stereographic rectification of the gridded area of a quarter-orbit. Note that the SSP track is tangent to the 80° circle of latitude. The region ABDC is drawn for the northern hemisphere, where the satellite travels from E to F. Returning to the assumptions regarding these results, assume that the earth's rotation is

considered. Then each scan line covers a portion of the earth slightly westward of the preceding line. The net effect is to cause the entire region to be more "slanted." However, the net area viewed--say, in square miles--will remain the same (in the same way that the area of a parallelogram is equal to that of a rectangle where the heights and lengths are equal). The assumption regarding the forward motion of the satellite while it is scanning also leads to no change in area. If attitude errors are present, then the area viewed does change very slightly, but the percentage change is nil.

The shape of the polar stereographic region in the southern hemisphere, when the satellite approaches the pole, is the same as in Fig. 18. However, when the satellite is moving to the north, then the polar stereographic region is the mirror image of that in Fig. 18. In any event, the areas of these projections are also the same.

2. The (Unrectified) MRIR Source Picture

In the source picture each scan line, caused by one mirror rotation, corresponds to one line in the picture. Each equal mirror angle, at the satellite, corresponds to one element along each line. For a quarter-orbit, the size of the source picture is as follows: The resolution of an MRIR device is 2.8°. In the total viewing angle of 109° there are, therefore, (109°/2.8°) = 39 elements in each scan line. At this angle of 2.8°, and for an altitude of 500 nm, the resolution element at the SSP track covers an area 24.4 nm by 24.4 nm. If, along the SSP track, the mirror revolves at such a rate that there are no overlapping lines, or gaps between lines, then there will be (5,400/24.4) = 220 lines in a quarter-orbit. There are thus (220) (39) = 8,580 data elements in the source picture.

3. Relationship Between the Source Picture and the Polar Stereographic Rectification

It is assumed that there will be no overlap of data when the source picture is rectified to a polar stereographic projection. The minimum magnification of a polar stereographic projection occurs about the pole. It is assumed that there will be no overlaps in this region,

but it is also assumed that there will be no gaps. Thus, the source data are given no scale change when mapped into this area. In Fig. 18, the minimal scale factor is applied in the vicinity of point E. At point E the size of each target element is thus set at 24.4 nm by 24.4 nm. Since the distance from A to B is 1720 nm, there are (1720/24.4) = 71 target elements from A to B. The source picture has only 39 elements in this same arc. In Fig. 18, the distance GH is 39/71 of the distance AB. Since there are 220 lines in the source picture, the distance GI is equal to 220/39 of the distance GH. The area GHJI is therefore the size of the unrectified source picture that corresponds to ABDC.

The area of each of the two regions is determined; and the resultant ratio of the areas is 2.986 to 1.0. There are therefore approximately three times as many target elements as there are source elements.

If the polar map, in Fig. 18, is magnified so that there are 10 elements per inch, then the radius of the resulting map (pole to equator) will be 28 inches. Reference to Fig. 14 shows that the values of the individual elements can be easily read at this scale. If a polar stereographic mosaic is made from successive swaths, then the diameter of the resultant map will be 56 inches, or 4 ft. 8 in.

4. Formatting the Rectified Output

If the target picture is printed so that there are 10 elements per inch, then this picture will be about 28 inches long and about 14 inches wide (at the widest point) as shown in Fig. 21. In a typical facsimile device, the size of the paper used is 8 1/2 by 11 inches. Allowing for margins, it is assumed that the target picture will be printed as 8- by 10-inch pictures. This means that several sections will result for one quarter-orbit. The manner in which the sections are arranged is somewhat arbitrary. Each line of numbers on the target picture is parallel to the lines printed by the facsimile machine. It is assumed that the 8-inch side of the output section will be parallel to the lines of data. In Fig. 21, a feasible format is shown by the dotted lines. With this arrangement, a quarter-orbit results in six individual sections, which can then be joined.

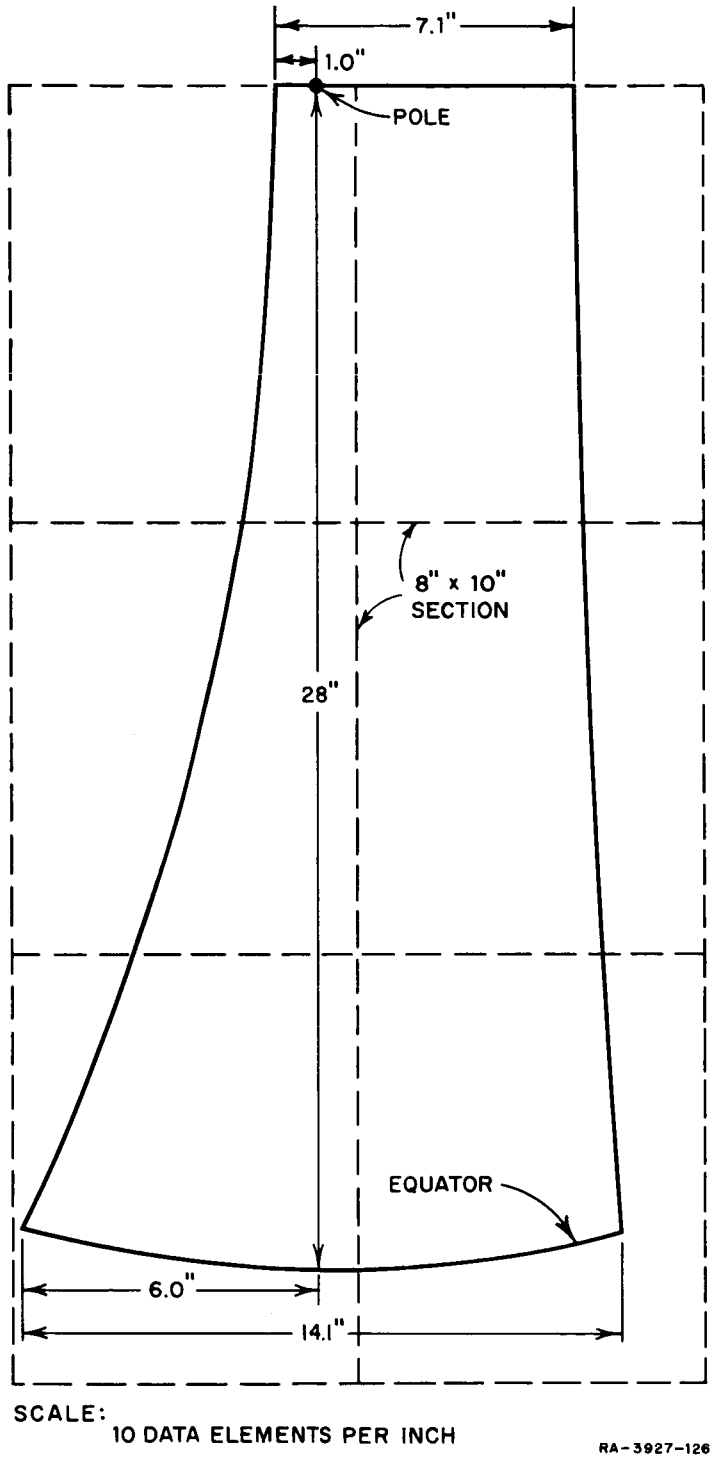

FIG. 21 APPROXIMATE DIMENSIONS AND OUTPUT SECTIONING FOR A QUARTER-ORBIT

5. Gridding the Data Elements

There are two basic methods for indicating the location of a grid point, depending on the accuracy to which it is computed. The resolution of a data point near the SSP track is 24 nm. For some purposes it may be sufficient to locate a grid point to a similar accuracy. An example of a data point without a grid point is shown in Fig. 22(a) (see also Fig. 15). Figure 22(b) shows how the entire data element can be changed to indicate the presence of a grid point that is somewhere within that area. Other background patterns, such as a checkerboard, can also be used. It is desirable, from a hardware point of view, to use only the same gray levels as in the normal data element.

If the grid point is calculated to a higher accuracy, then a format such as in Fig. 22(c) can be used to indicate the grid point location. The facsimile printer will normally have a "printing resolution" of 100 elements per inch. If 10 MRIR data points are printed per inch, then each such data point will occupy an area containing 10 by 10 "printing resolution" elements. Near the SSP track, a data point covers an area of 24 by 24 nm. Thus each "printing resolution" element corresponds to an area of 2.4 by 2.4 nm. Grid points can thus be indicated to an accuracy of 2.4 nm. If only 5 MRIR data points are printed per inch, then a grid accuracy of 1.2 nm can be indicated.

FIG. 22 INDICATING A GRID POINT IN A DATA ELEMENT

F. The Exact Rectification Method

In this method, the source picture can be rectified to any desired degree of accuracy. The satellite attitude errors are taken into account in an exact way; as a result, the magnitude of such errors does not reduce the accuracy of the rectification. The method consists of three steps as described below.

1. Step 1

The latitude-longitude coordinates of each target element are determined for a map such as in Fig. 18. It is assumed that the longitude of point F is 0°. In this example, point F is the intersection of the SSP track and the equator. (As noted previously, the calculations involved in this step are performed only once for any given map projection.)

2. Step 2

The source picture is gridded using any feasible gridding method. Two such methods have been developed for the HRIR pictures, where exact account is taken of any attitude errors. With slight changes in constants, each can also be used for the MRIR pictures. The grid "spacing" that should be used is determined in Step 3. In the HRIR system, the spacing used was 2° in latitude and 2° in longitude. The accuracy of the rectification procedure is related to the grid spacing used, where a smaller spacing yields a more accurate target picture. However, smaller grid spacings will result in a somewhat longer computing time to obtain the grid points. It is not necessary to determine the latitude and longitude of any other elements in the source picture. (If desired, these coordinates can be obtained by interpolation from the gridded elements; however, as described below in Step 3, this calculation is unnecessary.)

After the picture has been gridded, the longitude of the SSP track crossing with the equator is determined. This longitude value is then subtracted from the longitude value of each grid point.

3. Step 3

In this step, each target element is located in the source picture. The nearest source element is identified and its value is transferred to the desired target element. This process continues until all the target elements are filled. The nearest source element is located using linear interpolation. This location procedure is explained by means of a numerical example.

Assume that it is desired to determine the value of the target element, where w = 160 and z = 73; that is line number 160 and element number 73 within this line. Let the latitude and longitude of this element be 28.3°N and 11.2°W. Assume that the source picture has been gridded at 2° intervals. It is then necessary to locate on the source picture the four grid points: point 1 = (30.0°N, 12.0°W), point 2 = (30.0°N, 10.0°W), point 3 = (28.0°N, 12.0°W), and point 4 = (28.0°N, 10.0°W). Each of these points has been gridded in Step 2.* Each of these points has a u and v coordinate in the source picture, where u is the line number and v the element number within the line. Assume that the u, v coordinates for each of the four grid points is as follows: (201,20), (198,27), (207,21) and (204,29), respectively. (These u, v numbers and w, z numbers are chosen to only illustrate the procedure and do not necessarily have any relation to actual values.) In Fig. 23, these four grid points are displayed. The approximate location of the point (28.3°N, 11.2°W) is also noted as point 5.

* In general, the longitude values of the grid points will not be even multiples of 2°. As noted in Step 2, a constant is subtracted from all longitude values, and this constant may have any value. However, for ease in understanding the example, the reader can assume that this constant is, say, 40.0°.

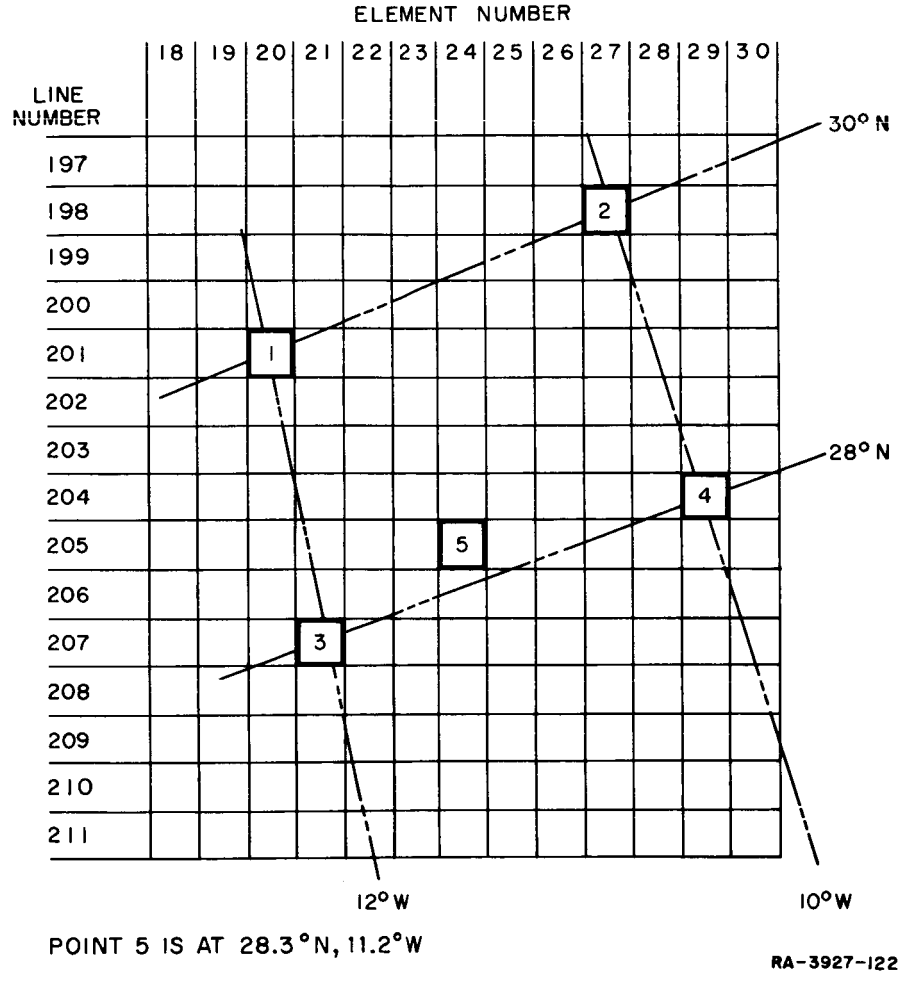

FIG. 23 LOCATION OF ELEMENTS ON THE SOURCE PICTURE

The u, v coordinates of the point (28.3°N, 11.2°W) are u = 204.90 and v = 23.99. These values are obtained from the following linear interpolation formulas:

$$u_5 = (1 - a - b + ab)\, u_1 + (a - ab)\, u_2 + (b - ab)\, u_3 + (ab)\, u_4 \quad (1)$$

$$v_5 = (1 - a - b + ab)\, v_1 + (a - ab)\, v_2 + (b - ab)\, v_3 + (ab)\, v_4 \quad (2)$$

where

(1) u_5 and v_5 are the coordinates of the desired target element; (u_1, v_1), (u_2, v_2), (u_3, v_3), and (u_4, v_4) are the coordinates of the four grid points immediately surrounding (u_5, v_5), such that their latitudes and longitude values "enclose" the latitude and longitude of the desired target element. (Note the latitude and longitudes in Fig. 23 as an example.)

(2) (u_1, v_1) is the "upper-left" point, (u_2, v_2) is the "upper-right" point, (u_3, v_3) is the "lower-left" point, and (u_4, v_4) is the "lower-right" point.

(3) a is the percentage difference in longitude that point 5 lies from 1 to 2, or from 3 to 4--in Fig. 23, a = 0.3/2.0 = 15%;

(4) b is the percentage difference in longitude that point 5 lies from 1 to 3, or from 2 to 4--in Fig. 23, b = 1.7/2.0 = 85%.

To derive the linear interpolation formula one locates the coordinates of a point that is a% of the distance from point 1 to point 2, and also the coordinates of a point that is a% of the distance from point 3 to point 4. One then locates the coordinates of a third point that is b% of the distance from the first calculated point to the second calculated point. The third calculated point is the desired one.

It is recommended that only linear interpolation be used to obtain the coordinates of the desired target elements. If the given formulas are not sufficiently accurate, then it is necessary to decrease

the grid spacing used in Step 2. For example, it may be necessary to locate every 1° latitude and longitude intersection. Note also that it is more accurate to save the exact location of every grid point rather than rounding-off to the nearest line number and element number. Rounding-off is only necessary when producing a hard-copy print.

In the given example the $\underline{u}$, $\underline{v}$ coordinates of the desired target element are u = 204.90, and v = 23.99. One then selects the value of element (205,24) and locates this value in the target picture whose element coordinates are w = 160, and z = 73. To fill just one target element thus requires about nine multiplications in Eqs. (1) and (2), and two divisions to obtain the values $\underline{a}$ and $\underline{b}$; in addition several additions and subtractions are necessary.

In the above procedure it is necessary to locate each target element into the source picture. This is quite a conservative approach and is necessary only if the slopes of the latitude and longitude lines are changing extremely rapidly. A better approach would be to locate, say, every other target element. The location of an intermediate target element would then be simply the average of the locations of its two adjacent elements. Depending on the accuracy required, one can extend this concept and locate, say, every tenth target element and obtain the location of the others by simple proportions. The advantage is obviously to further decrease the amount of computer calculations per element. Each target location that is obtained by simple proportions would require only two multiplications.

4. Timing Estimate

Since the target picture for a quarter-orbit contains three times as many elements as the source picture, there are 25,740 target elements. To obtain the x, y coordinates of each target element requires eleven "equivalent multiplications,"* where each such "equivalent multiplication" takes 300 micro-seconds on the CDC-924. To rectify all the target elements will require (25,740) (11) (300 micro-seconds) = 84.9 seconds. To rectify a complete orbit would then require about 6.4 minutes. Added to this is about another minute of computing time necessary to grid the source picture, if a 2° spacing is used.

These computing times are for only one channel. There are, in total, five MRIR channels. However, each of these channels views the identical portion of the earth at the same time. Therefore, their grids and rectifications are identically the same. The total time to grid and rectify all the MRIR channels should be within 10 minutes.

In the above, it is assumed that each target element will be transferred into the source picture. It does not appear that this degree of precision is necessary. It is sufficient in many portions of the target picture to transform every other element. The transformed coordinates of the remaining target elements are obtained by a simple average. Upon further examination, it may be possible that even fewer elements need be transformed. It is thus estimated that the 10-minute computing period is a high upper bound.

---

* "Equivalent multiplications" are used to estimate computer time required. Multiply and divide each are counted as one equivalent multiplication. Evaluation of a trigonometric function is counted as eight and finding a square root as five equivalent multiplications. The number 8 is based on the use of efficient polynomials that would average eight multiply and divide operations and 5 is based on the use of Newton's method, averaging five multiplications and divisions. In this method logical instructions, add, subtract, store, etc., are accounted for by the assumption that equivalent multiplication represents 10% of the total computing time. The total number of equivalent multiplications is multiplied by 300 microseconds to obtain total computing time. Actually, the CDC 924 multiply time is 27.9 microseconds or less, depending on the number of ones in the multiplier.

G. The Tabular Rectification Method

For some purposes it may be reasonable to assume that the satellite attitude errors and altitude variation can be ignored. It is anticipated that the actual attitudes will be within ±2.0°, and that the altitude will be within ±30 feet. Each such "departure" will result in a data location error of less than 24 nm--which is the size of a resolution element. If the satellite "departures" are ignored, then the target elements and the grid points will not be inaccurate by more than one resolution element.

For these assumptions, a particularly simplified rectification method can be developed, which consists of two steps: the first step results in a gridded source picture; the second is the rectification to the target picture.

The gridding process, performed in the first step, is not a necessary operation prior to rectification, although it is desirable that the grid points be present in the target picture. It is necessary, though, to compute the longitude of the point where the SSP track intersects the equator. The longitude of this point is denoted as λ_o.

The gridding method used is a particularly simple one. Since the attitude errors are assumed to be zero, and the altitude is assumed to be constant, then the latitude and longitude of each source element is only a function of the heading angle, the longitude λ_o, and scan-line number. The heading angle is always constant for any given quarter-orbit, and changes only slowly from one orbit to another. The latitude-longitude values of each source element can thus be easily determined. In particular, the latitude value of each source element is only a function of the line number and the element number within a line. (The latitude value is independent of λ_o.) The longitude value of each source element is a function of the line number, the element number within the line, and λ_o. The dependence on λ_o is, however, only that of an additive constant. That is, the longitude is determined for the case where λ_o is equal to zero. To the value thus obtained, the value λ_o is added. The elements closest to the desired latitude-longitude positions are then selected as the desired gridded elements.

The rectification procedure, in the second step, consists of a simple table look-up type of operation. If the longitude value λ_o is subtracted from any given quarter-orbit, then the resultant quarter-orbit would be identical with any other quarter-orbit. The rectification for each quarter-orbit is then also the same. One can thus construct a table for this purpose. The table is entered with the $\underline{x}$, $\underline{y}$ coordinate of each source element, and the $\underline{u}$, $\underline{v}$ coordinate of the corresponding target element is obtained. Each source element will be transferred to at least one target element; and in general a single source element will be transferred to several target elements. This table can be used as many times as desired, since the correspondence between the source picture and target picture is only a function of λ_o. (The only factor that would jeopardize the accuracy of the table is the constancy of the heading of the satellite, since it is based on a constant value of 80°.)

It is not possible to accurately determine the amount of computer time required without actually programming the method. However, it is estimated that a full orbit for all five MRIR channels can be gridded and rectified in about a minute using the CDC-924.

H. The Gridded-Tabular Rectification Method

This method is intermediate between the exact and the tabular methods. It retains advantages of each and is estimated to be reasonably rapid. Of the three methods, this method is particularly recommended for rectifying MRIR data.

Using the actual attitude errors, and the actual altitude, the source picture is accurately gridded using the same procedure as in the exact method. A calculated accuracy of 1 nm is easily obtained. After the grid points are located, the target elements are filled using the tabular approach. The net result is a rectified picture that closely approximates a polar stereographic and has grid points superimposed that are located very accurately.

The accuracy of the rectification will be within one resolution element--24 nm at the SSP track. And the accuracy of the grid points will be within 1 nm. These two statements relate to separate criteria

and should not be confused. The grid point accuracy refers to the relative accuracy between the position of target elements and the position of the grid points. Rectification accuracy refers to how closely the actual rectification compares with a true polar stereographic projection. In actual fact, the rectification error varies very little within a small region, because the satellite itself can only change its attitude slowly. Thus, shape distortions will be minimal within small areas; and this requirement is more important than the absolute amount of rectification error.

The high gridding accuracy does allow one to compare the MRIR pictures with HRIR, AVCS, or any other data. And as seen above, the lower rectification accuracy of this method is adequate. The grid points themselves can be presented as given in Fig. 22(c). In this way they can be depicted to greater accuracy than 24 nm resolution.

1. Location of Grid Points

It is not immediately obvious how one finds the position at which to enter a grid point into the rectified target picture. This problem is also present in the other two rectification methods; however, its presentation is more apropos in this method. Consider first the simpler situation where a grid point is calculated to an accuracy of 24 nm. This means that the nearest source element is identified as containing this grid point. The location of the grid point within the source element cannot be specified. When the source picture is rectified, a given source element may map into only one target element, or may map into several target elements. In the latter case, it is perfectly correct to indicate each one of the several target elements as a grid element. In a polar stereographic projection, the grid elements are shown as larger areas closer to the equator, because the projection is "stretched" in this region more than in any other region. Aesthetically, however, it would be preferable that only one target element be indicated as a grid element, irrespective of the amount of local magnification. In Fig. 24(a), a source element is shown that maps into three target elements. If this source element happened to contain a grid point, then

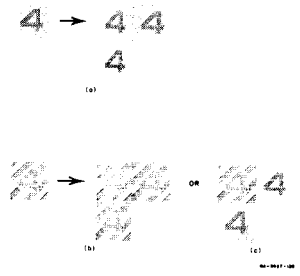

FIG. 24 INDICATING A TARGET ELEMENT CONTAINING A GRID POINT

it could be indicated as three grid elements in the target picture, as shown in Fig. 24(b). Preferably, only one of the three target elements would be selected as a grid element, as shown in Fig. 24(c). This single target element can be selected on an arbitrary basis. Another possibility would be to calculate the grid point location to an accuracy better than 24 nm, and so select the proper target element.

A situation more complex than that discussed above occurs when the grid point is calculated to an accuracy of about 1 nm. It is now necessary to select not only the proper target element, but to also indicate a location within this target element [as shown in Fig. 22(c)]. This is achieved by first gridding the source picture to the required accuracy. In this case, the location within a particular source element is noted--say, a Δx and a Δy offset from the center of the source element. These two quantities are expressed as percentages as shown in Fig. 25(a). Each source element has a corresponding area of coverage in the target picture. (In fact, this is how the tabular procedure is determined.) The corresponding area can be specified with four quantities: the $\underline{w}$, $\underline{z}$ coordinate of the center of the rectified square area; the magnification, $\underline{m}$, of the rectified square area; and the angular rotation, $\underline{\alpha}$, of the rectified square area. The exact location of the grid point can then be located in the $\underline{w}$, $\underline{z}$ coordinate system of the target picture as shown in Fig. 25(b).

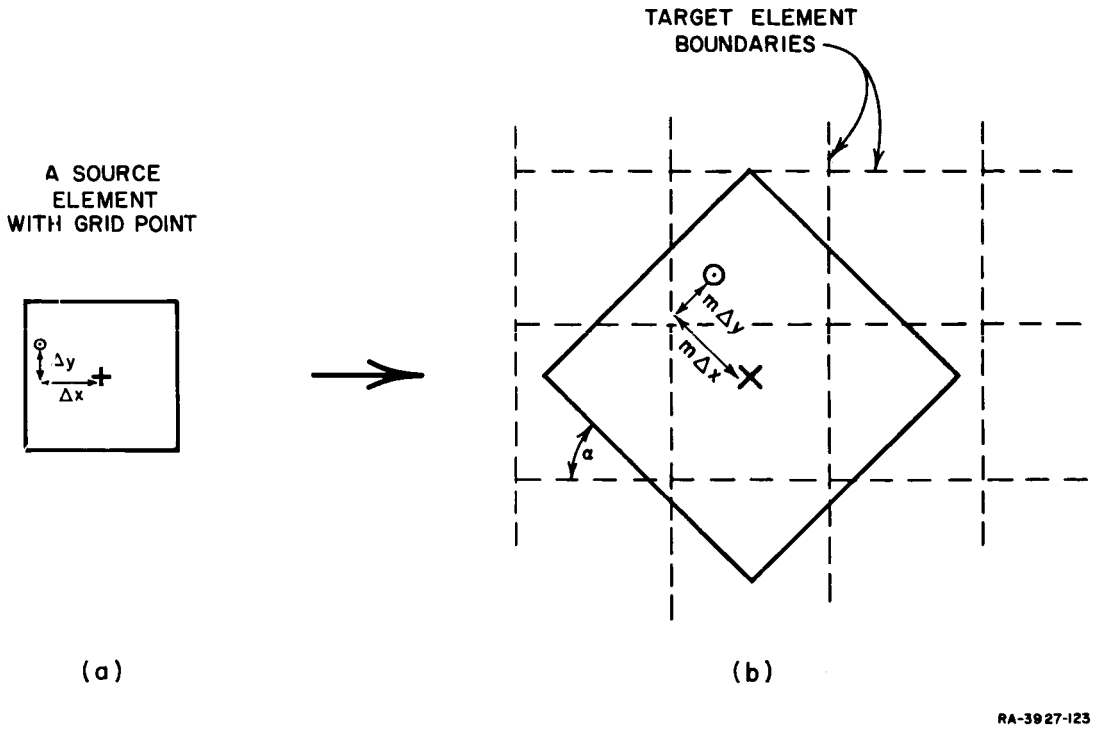

FIG. 25 POSITION OF A GRID POINT IN A TARGET ELEMENT

2. General Flow Chart

Based on the timing estimates for the exact and tabular methods, it appears that all five channels can be gridded and rectified in about 2 minutes using the CDC-924. A more accurate estimate would necessitate the construction of an actual computer program. A general flow chart of this method is given in Fig. 26 and is applicable to almost any general-purpose computer. A more detailed flow chart cannot be prepared without reference to a specific computer.

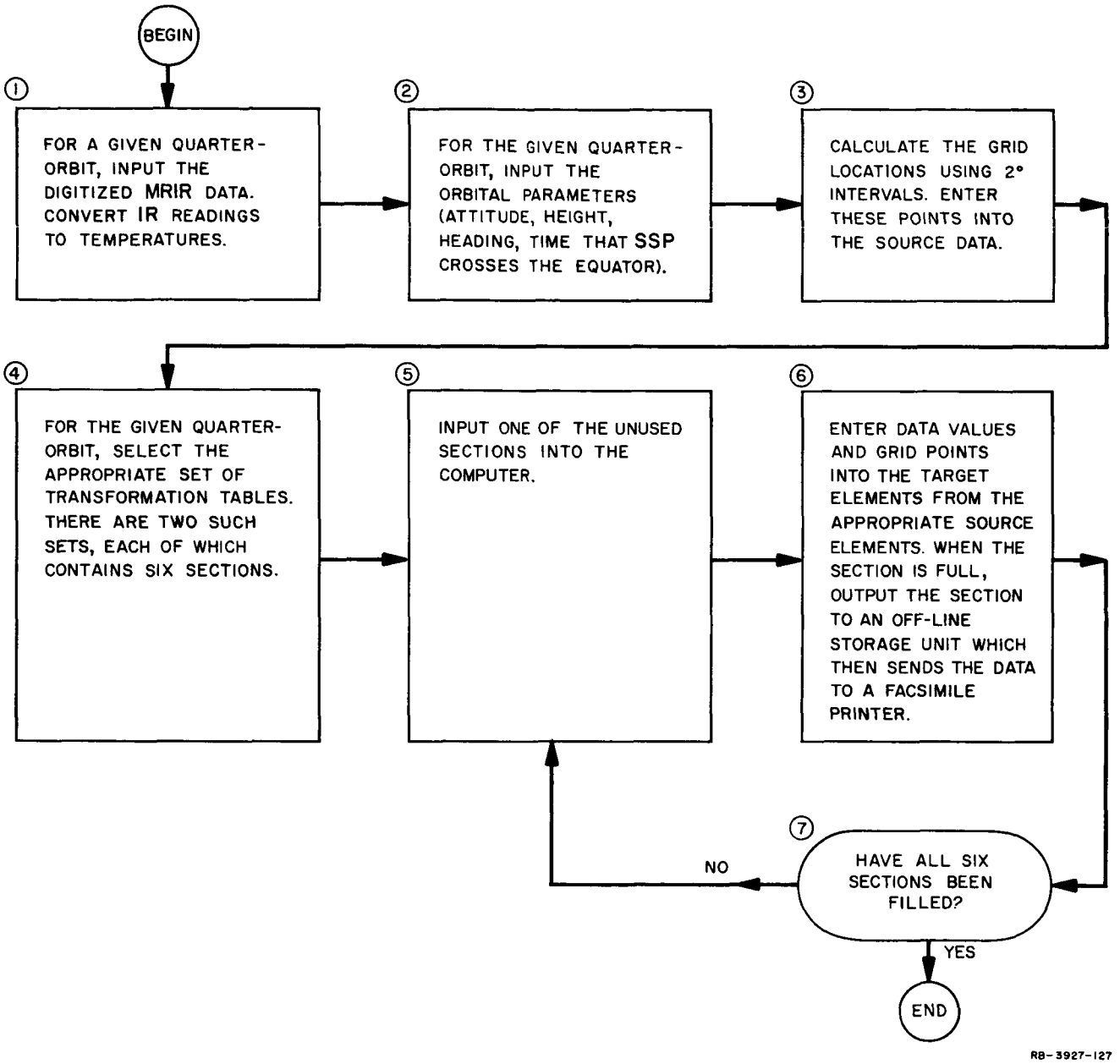

FIG. 26 GENERAL FLOW CHART FOR THE GRIDDED-TABULAR RECTIFICATION METHOD

The flow chart consists of seven functions, each of which is discussed below:

(1) Prior to entering the data into the computer, the MRIR analog signal must pass through an analog-to-digital device. The resultant digital data occupy (220) (39) = 8,580 addresses within the computer. Each address contains three items: (1) a $\underline{u}$ value, where u = 1, 2,...,39; (2) a $\underline{v}$ value, where v = 1, 2, ..., 220; and (3) an IR reading. Using a suitable formula, the IR readings are converted to temperatures, where the temperature is then rounded-off to the nearest 10°K. The set of possible temperatures is 200°K, 210°K, ..., 320°K. Once the temperature is determined, the original IR reading is no longer stored.

(2) Sufficient information must be entered here so that the grid points and the longitude λ_o can be computed. This longitude is the point at which the SSP track crosses the equator. These calculations require specification of the time and location of the satellite for the given quarter-orbit.

(3) The source picture is gridded using 2° grid points. Near the pole, a somewhat greater spacing is used, similar to the HRIR grid pattern. A grid point is located according to the $\underline{u}$, $\underline{v}$ coordinate system in the source picture. If the grid points are calculated to a 24-nm accuracy, then it is only necessary to indicate whether or not a source element contains a grid point. If the grid points are calculated to a 1-nm accuracy, then it is also necessary to indicate the quantities $\Delta x, \Delta y$, $\underline{m}$, and $\underline{\alpha}$ for the source element.

(4) There are two sets of transformation tables corresponding to the four quarter-orbits. Each set is composed of six sections, similar to that shown in Fig. 21, where each section corresponds to an 8- by 10-inch output picture. An output picture has 10 data points per inch. There are thus (80) (100) = 8,000 data points per section. As can be seen in Fig. 21, no one section is completely used; a maximum of about 6,000 data points need be filled.

(5) Any unfilled section may be entered next into the computer memory. Each such section contains 8,000 target addresses. Each target address contains one of two items: (1) the $\underline{u}$, $\underline{v}$ coordinates of a source data element, or (2) a blank entry.

(6) Each of the 8,000 target addresses is examined in turn. If the contents are blank, the program proceeds to the next target address. If a $\underline{u}$, $\underline{v}$ coordinate is present, then the proper source address is located. The temperature

value is transferred to the target address. If a grid point is present, its target position is also determined and transferred. When all the target addresses have been examined and filled, the entire section is read out to an off-line storage unit. This off-line unit acts as a buffer for the facsimile device.

(7) This is simply a branch command; it determines when the rectification process for a quarter-orbit is completed.

APPENDIX A

LIMB DARKENING

1. Introduction

When utilizing radiation data it will frequently be desirable--if not necessary--to apply corrections for absorption of radiation by such atmospheric constituents as water vapor, ozone, carbon dioxide, transparent cirrus, and particulate matter. For example, in the case of the window channel for TIROS II, the differences between the measured effective blackbody temperature, Te, and the actual surface (cloud or ground) temperature, Ts, varied between zero at lower Te values (high cloud top surfaces) and 10°C at higher Te values (warm earth surfaces). In this example, however, the differences refer to viewing in the nadir direction only. Another possible correction factor which should be considered is the so-called limb darkening, which for ease of discussion will be defined* here for the window channel as the difference, ΔTe, between the effective temperature from the nadir direction to that which would have been measured from an arbitrary direction (see Fig. A-1).

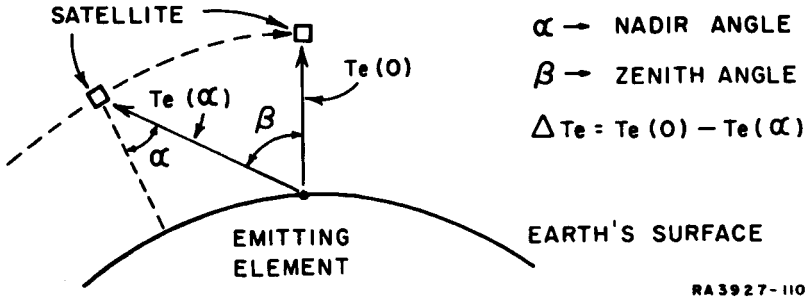

FIG. A-1 ILLUSTRATION OF LIMB DARKENING

* Generally it has been defined as the ratio or difference of intensity or flux rather than in terms of effective temperature.

Now the variation of ΔTe with the nadir angle is, of course, due partially to the increase in the atmosphere (and consequently the amount of water vapor, etc.) which must be traversed. In the case of TIROS II Channel 2, the extreme differences of ΔTe for this reason approached 10°C (or a total difference between Te and Ts of about 20°C). Another reason for an increase of ΔTe with increasing nadir angle is an effective change in the surface such as occurs for partial cloud cover conditions, and in particular for those conditions produced by cumulus activity. This increase in ΔTe arises because of the vertical thickness of the cumulus clouds as illustrated in Fig. A-2.

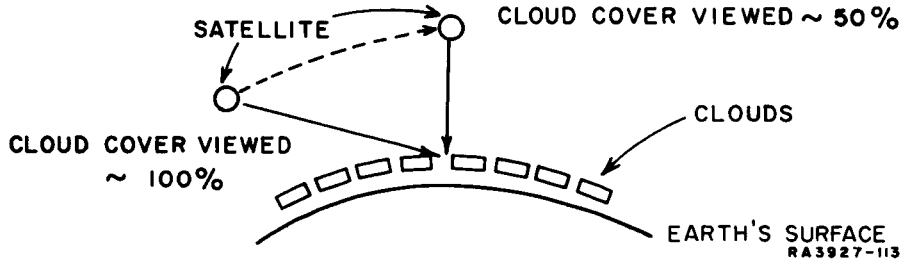

FIG. A-2 ILLUSTRATION OF PARTIAL CLOUD COVER EFFECT

Because these two causes of limb darkening (increased optical path length and effective variation or change in surface observed, such as for partial cloud cover) are somewhat different in nature, the degree and significance of each will be discussed separately.

2. Limb Darkening--Increased Atmospheric Path Length

In this section, the cloud cover conditions will be restricted to either clear or overcast because, as mentioned, partial cloudiness produces considerable complexity. With this stipulation, the limb darkening effect is largest for clear and low overcast conditions or for high water vapor and temperature lapse rates--characteristic of low latitudes. The effect is smallest for high overcast skies or for low water vapor and temperature lapse rate--prevalent at high latitudes.

Wark et al.[6] have conducted theoretical investigations for these limb darkening corrections with respect to the first three TIROS satellites. Based on their 1962 equations[6], the following tabulation (Table A-1) has been constructed.

Table A-1

APPROXIMATE LIMB DARKENING EFFECT (ΔTe) FOR TIROS III, CHANNEL 2

Nadir Angle	Effective Temperature			
	250°K	270°K	290°K	310°K
25°	0°	0°	0°	0°
40°	0°	0°	1°	2°
50°	0°	0°	2°	4°
60°	0°	2°	4°	10°

As one would expect, for the window channel it is only noticeable when both a very high temperature (peculiar to locations such as North Africa) and a very large nadir angle are considered. The importance of limb darkening under these latter-mentioned extreme conditions was demonstrated by Larsen et al.[17] in 1963.

In the case of the Nimbus where a narrower and clearer window is to be utilized, the limb-darkening effect should be even less. In addition to this, some of the higher nadir angle data are expected to be discarded since the data are duplicated during adjacent passes with a lower nadir angle view. Therefore, it may be concluded that the effect of limb darkening in the window channel--excluding partial cloud cover effects--will be small and at this stage not an important consideration. Continued investigations and research are needed, however, and particularly for the other channels, such as Channel 4, where it is several times more effective.

As a corroboration to the above considerations, a statistical investigation was performed with data from portions of three TIROS III passes, Nos. 29, 44, and 101. In this investigation, the warmer (>270°K) and the colder temperatures (<250°K) were read into the Burroughs 220 computer, and the average temperature versus nadir angle obtained (Fig. A-3). As anticipated, the cold curve (representative

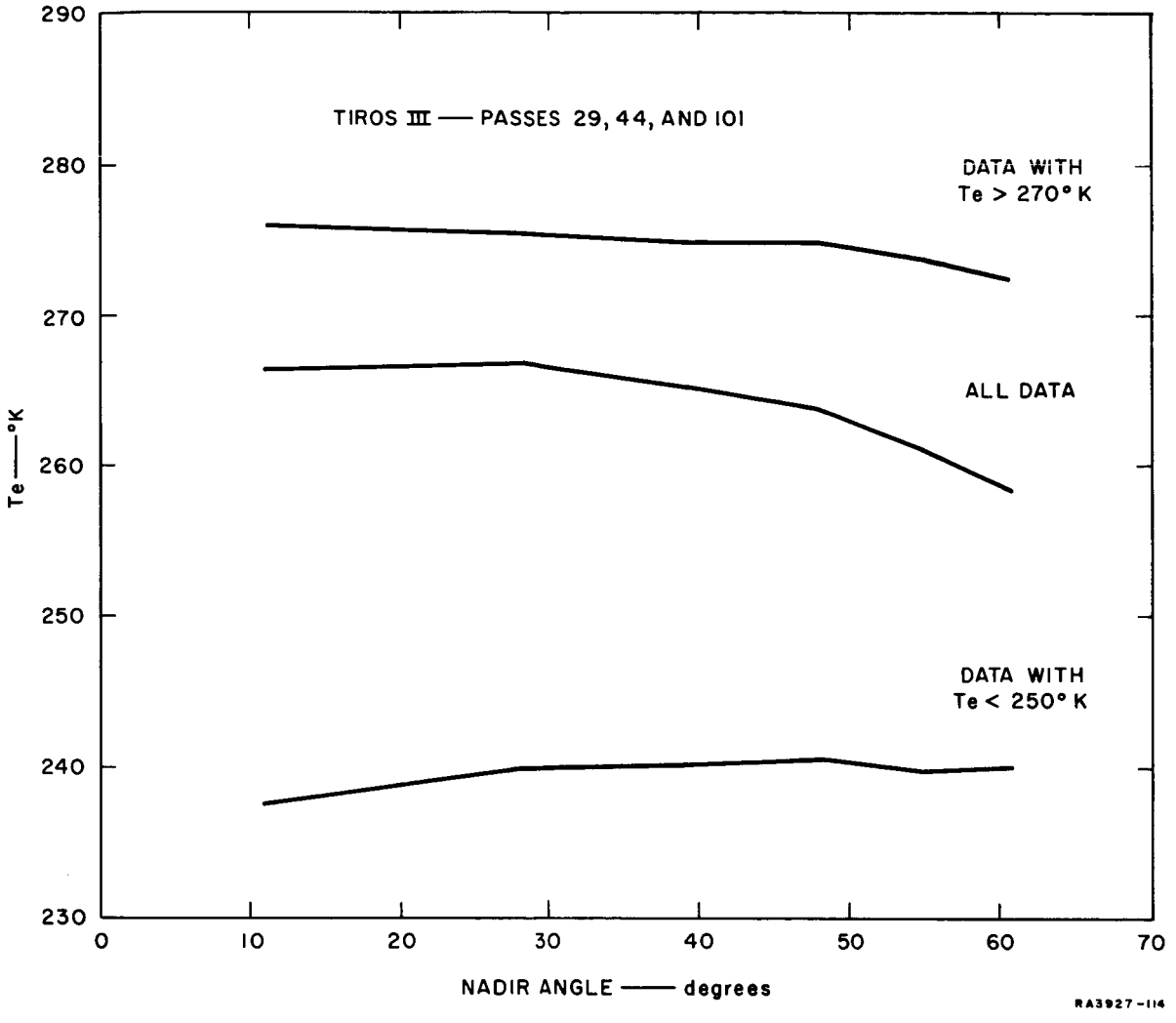

FIG. A-3 AVERAGE EFFECTIVE TEMPERATURE VERSUS SATELLITE NADIR ANGLE

of high overcast conditions) showed no suggestion of limb darkening. Also, in agreement with the preceding discussion, the warm curve (representative of clear conditions) showed a limb darkening effect of 3-4°C. A curve which included all data is also presented, and exhibits an average limb darkening decreases with increasing nadir angle of up to 8°C. This is to be expected because the data included partial cloud cover conditions which will now be considered.

3. Limb Darkening--Partial Cloud Cover

Although the variation in cloudiness from the zenith to the horizon--due to the perspective involved--is an age-old problem, very few investigations have been performed in order to describe its degree or nature. As early as 1922, Lindholm[18] measured this effect at Ilmala, Finland, during the summer half of the year. The results in terms of the average percent cloudiness are illustrated in Fig. A-4.

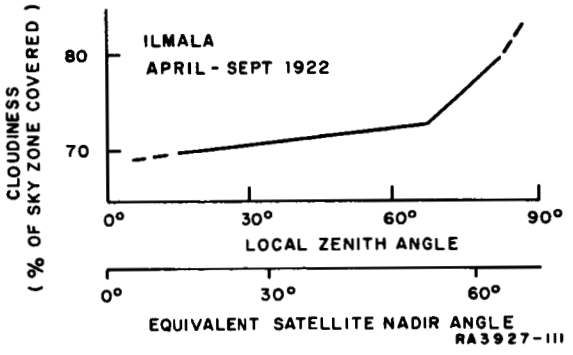

FIG. A-4 CLOUDINESS VERSUS ZENITH ANGLE

The cloudiness was found to vary from 70 percent near the zenith to 80 percent near the horizon, with a total average cloudiness of 74 percent. As can be seen in the illustration, the major change occurred near the horizon. Similar (more detailed) investigations throughout the world would be quite valuable, but to the knowledge of the authors, such investigations have not been performed. In 1962 Appleman[19] reported that he had found, by comparing surface observations with aircraft observations made simultaneously in the western United States during April 1961, that the surface observations of low cloud cover

were on an average, 14 percent too high; the average low cloud amount was 48 percent. No discrepancies were found for the medium or high cloud cover cases. As would be expected, this low cloud cover result (14 percent too high) is about three times larger than that suggested by Lindholm's results[18] (4 percent too high) which applied to total cloud cover. These two investigations at least indicate the general effect of partial cloud cover conditions. The total average curve of Fig. A-3 (computed from TIROS III, Channel 2 data) also appears to include a similar cloud effect error on cloud reading and varying with the angle of view.

In addition to the results presented in Fig. A-3, computations were made of the average values of the data for Passes 29 and 44 divided into temperature quartiles and separated according to whether the scan was directed to the north or to the south. The results proved to be subjected quite strongly to the prevalent synoptic situation; Pass 29 occurred about one day earlier and orbited about 5° higher (latitude) than Pass 44 (Pass 101 occurred about a day later than Pass 44, but covered a similar area). Due to the strong synoptic influence on the distributions, one would indeed desire more data than was available from these three passes to work with. Nevertheless, the results presented in Fig. A-3 are believed indicative of limb darkening, because they tend to avoid the complex synoptic situations brought on by partial cloudiness and in the case of the total average curve include sizable data samples. Wexler[20] also has reported (1963) a statistical investigation of limb darkening, but for TIROS II. His results--based on 70 orbits--appear to show a somewhat stronger limb darkening effect than does the total average curve of Fig. A-3; otherwise they were in general agreement.

One general outcome of this investigation is that the limb darkening which includes partial cloudiness does appear significant (roughly 10° on an average and even much greater under certain cumulus conditions), although it may be minimized (about one-half) by cropping the data with nadir angles greater than about 55°, as is tentatively

intended. An average correction might be applied, but it would introduce error about as frequently as it would eliminate it. Therefore, in order to correct properly for the limb darkening effect of partial cloudiness, it would be necessary to know beforehand the type of the sky cover; Blackmer and Alder[21] suggest (1963) that corrections in this way may be possible. An objective method of correcting may be possible in the future by utilizing multiple channels or other means to determine the cloud type. At present, however, it would require subjective inspection of the AVCS cloud photographs.

APPENDIX B

SCATTERING ANGLE COMPUTATION

1. Trigonometric Relationships

The computation of the scattering angle (and other relevant parameters) is primarily determined by a consideration of basic spherical trigonometry. Therefore, several relationships pertaining to oblique spherical triangles--to be used throughout this discussion--will now be stated without proof: They are:

$$\frac{\sin a}{\sin A} = \frac{\sin b}{\sin B} = \frac{\sin c}{\sin C} \qquad \text{(B-1)}$$

$$\cos a = \cos b \cdot \cos c + \sin b \cdot \sin c \cdot \cos A \qquad \text{(B-2)}$$

$$\frac{\cos\left[\frac{(a-b)}{2}\right]}{\cos\left[\frac{(a+b)}{2}\right]} = \frac{\tan\left[\frac{(A+B)}{2}\right]}{\cot\left(\frac{C}{2}\right)} \qquad \text{(B-3)}$$

where A, B, and C are the three angles (in degrees) and a, b, and c are the opposite sides (also in degrees),as in Fig. B-1. The latter equation, 3, is one of a number of relationships known as Napier's analogies. Also it should be noted that Eq. (B-1) is not unique, but may be used unerringly if the unknown angle always lies between 0° and 90°.

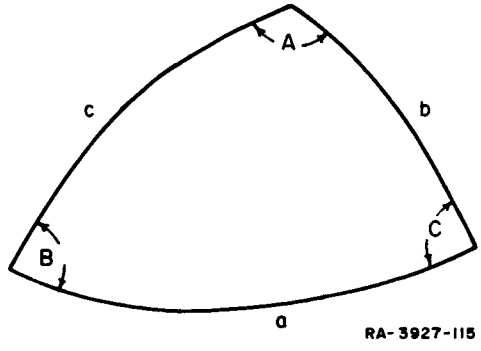

FIG. B-1 ARBITRARY OBLIQUE TRIANGLE

2. The Scattering Angle

In the following discussion, equations necessary to compute the scattering angle from data (satellite nadir and azimuth angles and latitude and longitude) provided by the Nimbus system will be derived. The geometry of the scattering angle is shown in Fig. B-2 for the case when the subsatellite point lies in the plane of the sun's vertical.* In this case

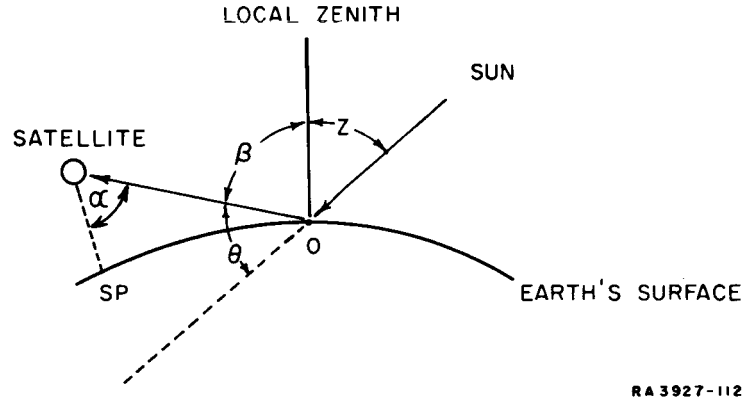

WHERE
- O is the scattering element
- SP is the subsatellite point
- z is the sun's zenith angle (from O)
- β is the satellite's zenith angle (from O)
- α is the satellite's nadir angle
- θ is the scattering angle

FIG. B-2 TWO-DIMENSIONAL ILLUSTRATION OF SCATTERING ANGLE

The scattering angle, θ, is equal to 180° minus the satellite's zenith angle, β, minus the sun's zenith angle, z. When the subsatellite point lies outside the plane of the sun's vertical, the geometry becomes more involved, as is illustrated in Fig. B-3. Here one may describe an oblique spherical triangle in space composed of the two sides, β, and z, and an included angle Φ. The scattering angle, θ, may be expressed by use of Eq. (B-2) as:

$$\cos (180 - \theta) = \cos z \cdot \cos \beta + \sin z \cdot \sin \beta \cdot \cos \Phi \qquad \text{(B-4)}$$

---

* The plane which contains the sun and the local zenith at the scattering element.

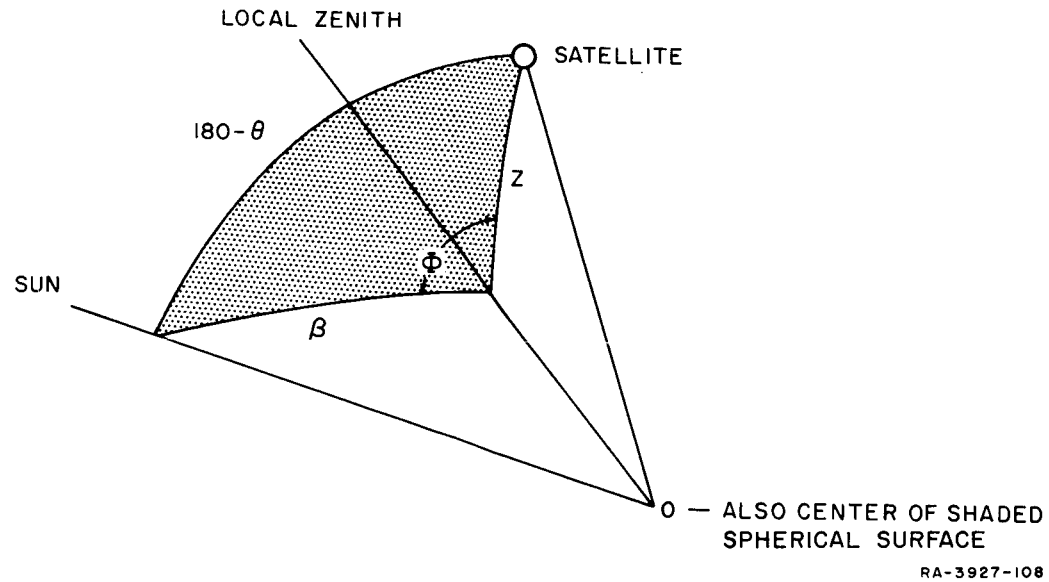

FIG. B-3 THREE-DIMENSIONAL ILLUSTRATION OF SCATTERING ANGLE

or if the sun's elevation angle, ϵ, is used instead of the sun's zenith angle, z, ($\epsilon = 90 - z$), Eq. (B-4) may be written as:

$$\cos\theta = -\sin\epsilon \cdot \cos\beta - \cos\epsilon \cdot \sin\beta \cdot \cos\Phi \ . \qquad \text{(B-5)}$$

It is now necessary only to introduce the values of ϵ, β, and Φ into Eq. (B-5) to compute the scattering angle.

The zenith angle of the satellite, β, is easily determined and is given by the relationship:

$$\beta = \arcsin\left(\frac{R + d}{R} \sin\alpha\right) \qquad \text{(B-6)}$$

where R is the earth's radius and d is the satellite's altitude (α is the satellite's nadir angle). The formula for the sun's elevation, ϵ, is given in several texts and is simply an application of Eq. (B-2):

$$\sin\epsilon = \sin\ell_o \cdot \sin\delta + \cos\ell_o \cos\delta \cos h_o \qquad \text{(B-7)}$$

where

ℓ_o is the latitude of the scattering element

δ is the sun's declination*

h_o is the local hour angle which is equal to h_G (Greenwich hour angle*) minus m_o (the longitude of the scattering element--west longitude being negative).

3. Determination Of Φ

The determination of Φ (which may be projected onto the earth's surface) may be seen in Fig. B-4, which displays the various angles involved in its computation. As can be seen from Fig. B-4, Φ equals $360° - SA - \chi$. Because Φ is to be used within a cosine, a more general equation may be written:

$$\Phi = SA + (\pm\chi) \tag{B-8}$$

The sign of χ (positive to the west) is determined in the computation of χ for which Eq. (B-3) may be used, that is:

$$\chi = 2 \operatorname{arcot} \left(\tan\left(\frac{PA + \Delta m}{2}\right) \frac{\cos\left(\frac{PO + (90-\ell_o)}{2}\right)}{\cos\left(\frac{PO - (90-\ell_o)}{2}\right)}\right) \tag{B-9}$$

where PO is the great circle angular distance between O and SP which is equal to $\beta - \alpha$.

It is now necessary to formulate the equations for the Δm and SA; PA (the satellite's azimuth) being considered a known quantity. The meridional difference between the subsatellite point and the observed point, that is, Δm, is found by Eq. (B-1), and is

$$\sin \Delta m = \sin (\beta - \alpha) \frac{\sin PA}{\cos \ell_o} \tag{B-10}$$

where Δm must be less than 90° (this will not hold for cases where the poles are crossed, for which a 180° change occurs).

* The sun's declination and the Greenwich hour angle for specific days and times are given in The Air Almanac.

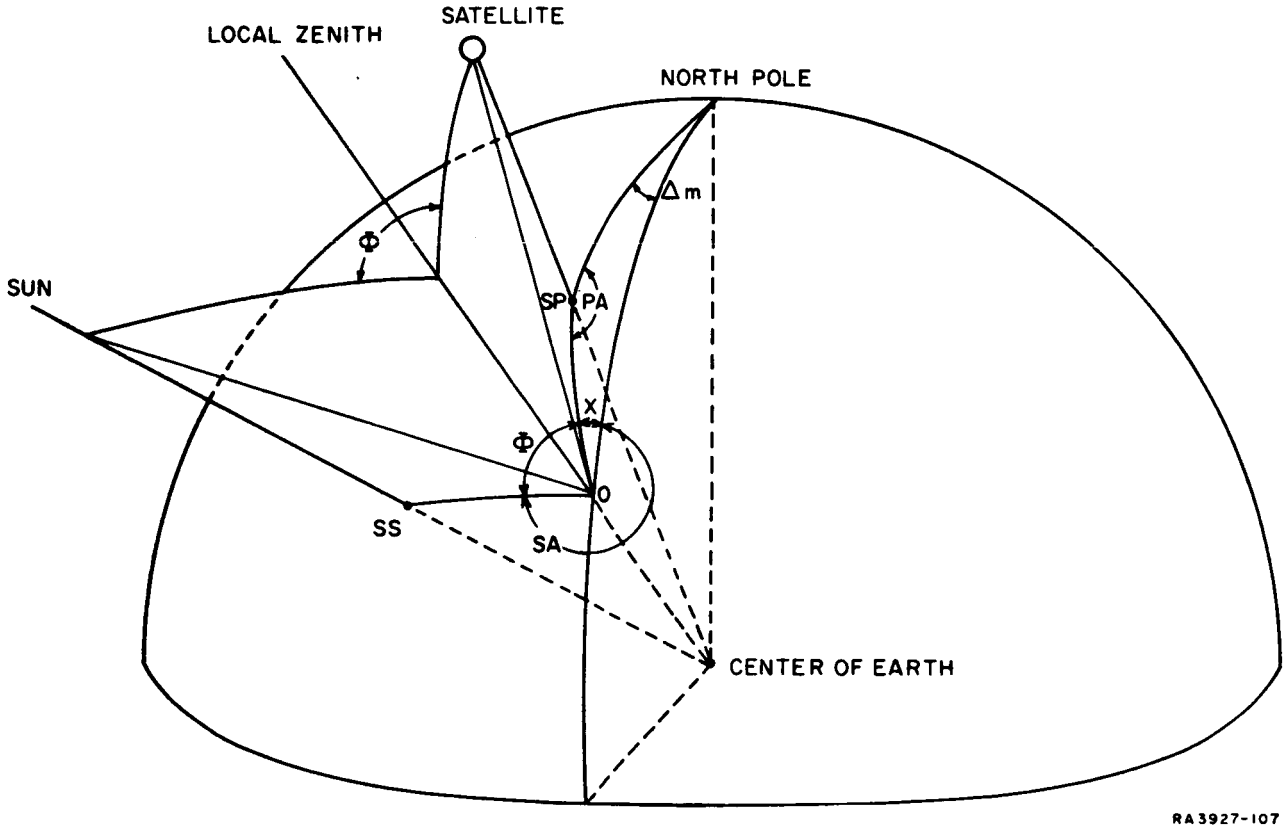

WHERE: SS Is the subsolar point
SA Is the sun azimuth
PA Is the satellite's azimuth as defined for the TIROS system
Δm Is the longitudinal difference between the scattering element and the subsatellite point
X Is the angle which relates Φ and SA with PA and Δm

FIG. B-4 ILLUSTRATION OF ANGLE Φ - 90° < PA < 180°

4. Sun's Azimuth

The sun's azimuth, SA, can be obtained through recourse to Napier's analogies and inspection of Fig. B-5. In terms of δ, ℓ_o, h_o, an angle TA may be defined as

$$TA = \arctan\left[\frac{\cos\left(\frac{\delta - \ell_o}{2}\right)}{\sin\left(\frac{\delta - \ell_o}{2}\right)} \cot\frac{h_o}{2}\right] - \arctan\left[\frac{\sin\left(\frac{\delta - \ell_o}{2}\right)}{\cos\left(\frac{\delta - \ell_o}{2}\right)} \cot\frac{h_o}{2}\right] \quad \text{(B-11)}$$

where

SA = TA if $\delta + \ell_o$ is positive

SA = 180 - TA if $\delta + \ell_o$ is negative and TA positive

SA = - (180 - TA) if $\delta + \ell_o$ is negative and TA negative

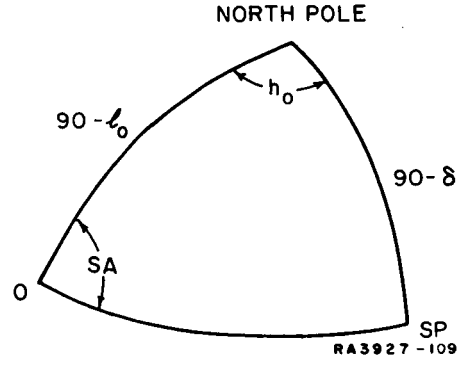

FIG. B-5 GEOMETRY FOR SUN'S AZIMUTH

5. Nimbus Orbits

The Nimbus satellite will circle the earth with an orbital plane inclined about 10° from the earth's axis. When the satellite passes the equator, it will be either local noon or midnight. A possible path which an ideal orbiting Nimbus satellite would describe across the rotating earth is indicated in Fig. B-6. From this path, specific satellite longitude, m_p, latitude, ℓ_p, and azimuths, PA, in addition to the sun's longitude, h_G, have been taken and used as input for a computer program (based on preceding discussion) to obtain θ (scattering angle) and ϵ (sun's elevation angle). With this input it is still necessary to generate the latitude and longitude of the observed point as determined by the nadir angles being considered. The latitude is given by

$$\cos \ell_o = \cos(\beta - \alpha) \cdot \cos \ell_p + \sin(\beta - \alpha) \cdot \cos PA \cdot \sin \ell_p \quad \text{(B-12)}$$

and the longitude is found by use of Eq. (B-10) already derived.

The results (θ and ϵ) obtained for a Nimbus orbit for $\delta = 0°$ have also been sketched roughly in Fig. B-6. Implicit in the figure is a scattering angle--versus Nadir angle--symmetry between the east and west scanning directions.

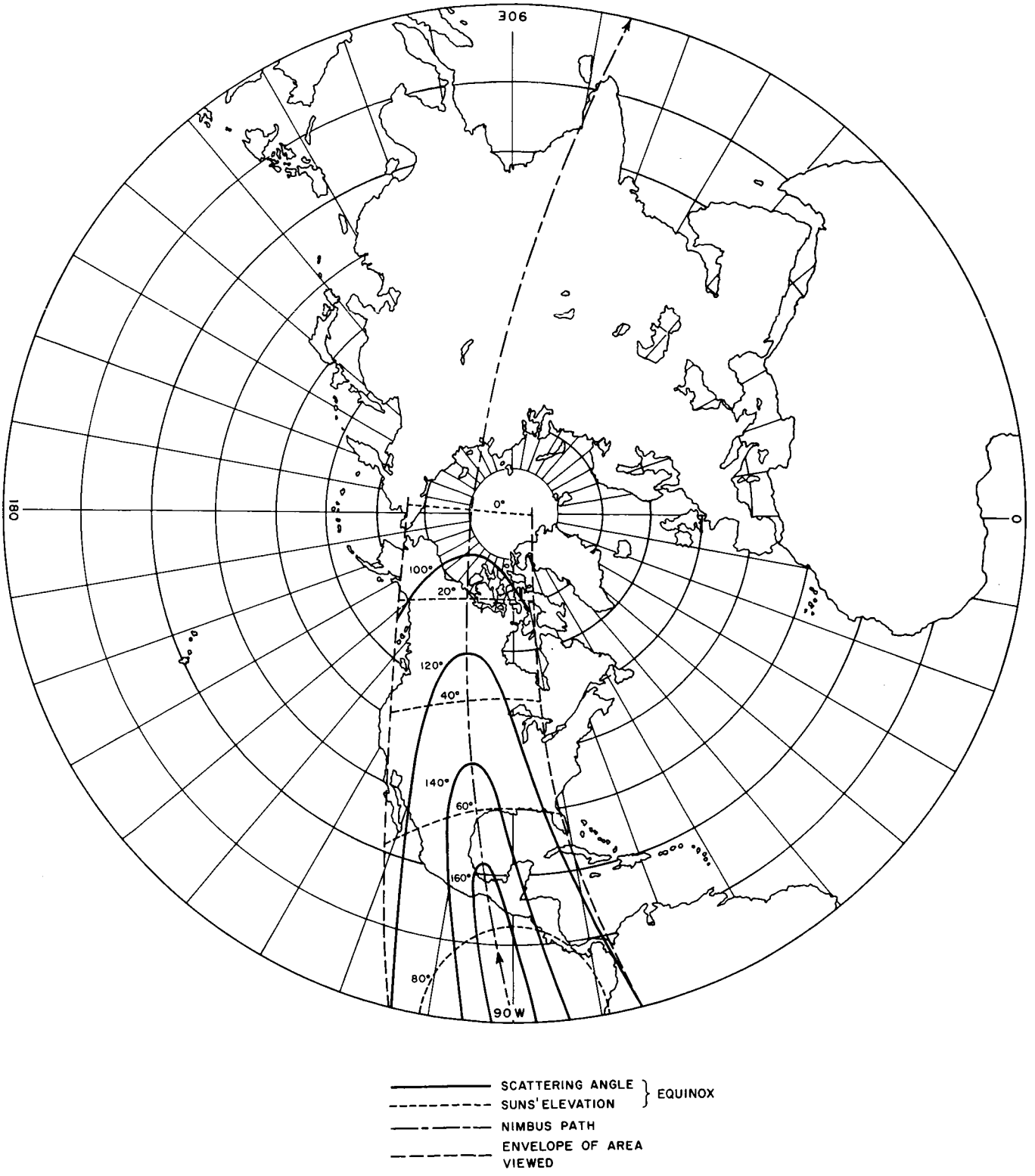

FIG. B-6 APPROXIMATE NIMBUS MRIR VIEWING CHARACTERISTICS

REFERENCES

1. W. R. Bandeen, R. A. Hanel, J. Licht, R. A. Stampfl, and W. G. Stroud, "Infrared and Reflected Solar Radiation Measurements from the TIROS II Meteorological Satellite," J. Geophys. Res. 66, 10, pp. 3169-3185 (October 1961).

2. R. A. Hanel and W. G. Stroud, "The TIROS II Radiation Experiment," Tellus 13, 4, pp. 486-488 (November 1961).

3. S. Fritz and J. S. Winston, "Synoptic Use of Radiation Measurements from Satellite TIROS II," Mon. Weather Rev. 90, 1, pp. 1-9 (January 1962).

4. P. K. Rao and J. S. Winston, "An Investigation of Some Synoptic Capabilities of Atmospheric Window Measurements from Satellite TIROS II," J. Atmos. Sci. 20, 1, pp. 12-23 (February 1963).

5. W. Nordberg, et al., "Preliminary Results of Radiation Measurements from TIROS III Meteorological Satellite," J. Atmos. Sci. 19, 1, pp. 20-29 (January 1962).

6. D. Q. Wark, G. Yamamoto, and J. Lienesch, "Infrared Flux and Surface Temperature Determinations from TIROS Radiometer Measurements," Meteorological Satellite Lab. Report 10, U. S. Weather Bureau, 84 pp. (August 1962).

7. National Aeronautics and Space Administration, TIROS III Radiation Data--User's Manual, 71 pp. (August 1962).

8. R. A. Hanel, "Determination of Cloud Altitude from a Satellite," J. Geophys. Res. 66, 4, p. 1300 (April 1961).

9. G. Yamamoto and D. Q. Wark, "Discussion of the Letter by R. A. Hanel--Determination of Cloud Altitude from a Satellite," J. Geophys. Res. 66, 10, p. 3596 (October 1961).

10. J. R. Blankenship, "An Approach to Objective Nephanalysis from an Earth-Oriented Satellite," J. Appl. Meteor. 1, 4, pp. 581-582 (December 1962).

11. W. Nordberg, "Research with TIROS Radiation Measurements," Astronautics and Aerospace Engineering (Volume devoted to "Weather Satellite Systems"), Vol. 1, No. 3 (April 1963).

12. M. H. Reese, "Brief Outline of the Method Used by Fleet Numerical Weather Facility to Draw Contour Weather Maps," Fleet Numerical Weather Facility, Monterey, California (April 1963).

13. R. C. Mach, "Research on the Processing of Satellite Photography by Digital Techniques," Final Report, Contract AF 19(604)-8432, Federal Systems Division, IBM, Kingston, New York (30 June 1962).

14. W. A. Marggraf, "Automatic Data Processing of Weather Satellite Data," Contract AF 19(604)-8861, General Dynamics/Astronautics, San Diego, California (31 January 1963).

15. R. M. Madvig, et al., "Nimbus Data Handling System," Second Quarterly Progress Report, Contract NAS5-1882, Stanford Research Institute, Menlo Park, California (July 1962).

16. R. M. Madvig, et al., "Nimbus Data Handling System," Third Quarterly Progress Report, Contract NAS5-1882, Stanford Research Institute, Menlo Park, California (October 1962).

17. S. H. Larsen, F. Petersen, and T. Fujita, "Evaluation of Limb Darkening and Total Infrared Flux Using TIROS III Radiation Data," presented at the 219th Meeting of the American Meteorological Society, Palo Alto, California (June 1963).

18. F. Lindholm, "Sunshine and Cloudiness in Sweden," Sveriges Meteorologiska och Hydrologiska Institut, Meddelander, Serie B, Nr. 11, 50 pp. (1955).

19. H. S. Appleman, "A Comparison of Simultaneous Aircraft and Surface Cloud Observations," J. Appl. Meteor. 1, 4, pp. 548-551 (December 1962).

20. R. Wexler, "Synoptic Interpretations and Heat Balance Determination from TIROS II Radiation Data," Scientific Report 1, Project 6698, Allied Research Associates, Inc., Concord, Massachusetts (January 1963).

21. R. H. Blackmer, Jr. and J. E. Alder, "Statistics of Cumuliform Clouds from U-2 Photographs," Final Report, Project 3892, Stanford Research Institute, Menlo Park, California (May 1963).

STANFORD
RESEARCH
INSTITUTE

MENLO PARK
CALIFORNIA

Regional Offices and Laboratories

Southern California Laboratories
820 Mission Street
South Pasadena, California

Washington Office
808–17th Street, N.W.
Washington 6, D.C.

New York Office
270 Park Avenue, Room 1770
New York 17, New York

Detroit Office
1025 East Maple Road
Birmingham, Michigan

European Office
Pelikanstrasse 37
Zurich 1, Switzerland

Japan Office
c/o Nomura Securities Co., Ltd.
1–1 Nihonbashidori, Chuo-ku
Tokyo, Japan

Representatives

Toronto, Ontario, Canada
Cyril A. Ing
Room 710, 67 Yonge St.
Toronto 1, Ontario, Canada

Milan, Italy
Lorenzo Franceschini
Via Macedonio Melloni, 49
Milano, Italy